# Experimental and numerical study of self-sustaining fluid films generated in highly compressible porous layers imbibed with liquids

Serguei Kunik, Aurelian Fatu, Jean Bouyer, Pascal Doumalin

# Experimental and numerical study of self-sustaining fluid films generated in highly compressible porous layers imbibed with liquids

Serguei KUNIK, Aurelian FATU, Jean BOUYER, Pascal DOUMALIN

*Pprime Institute, CNRS – University of Poitiers – ISAE ENSMA, UPR 3346, Mechanical Engineering and Complex Systems Dept., SP2MI, 11 Bd Marie & Pierre Curie, TSA 41123, 86073 Poitiers Cedex 9, France.*

**Keywords: Porous media, Numerical, Experimental, Thrust Bearing**

## Abstract

Ex-poro-hydrodynamic (XPHD) lubrication is a biomimetic-inspired lubrication mechanism consisting of self-sustained fluid films generated within highly compressible porous layers imbibed with liquids, whose solid phase induces compressive elastic forces that are negligible compared to the hydrodynamic forces generated inside the porous medium. This work focuses on the performance of XPHD lubrication in the context of tangential movement, adapted to the case of thrust bearings at low and medium rotational speeds. An in-depth study of a pre-selected porous material (polyurethane foam) was carried out in order to determine the physical characteristics and the crucial parameters for XPHD lubrication, namely the porosity and the permeability. The paper also proposes a theoretical and numerical model of XPHD lubrication. Classical lubrication assumptions are used, and flow within the porous medium is predicted using a new form of the Reynolds equation. A specially developed test rig allows for an experimental study of the XPHD lubrication mechanism. Finally, a comparison of the modeling and experimental results is presented.

## 1. Introduction

Generally speaking, a porous medium is a solid body that contains a certain quantity of regularly or chaotically distributed voids, which may or may not be connected to each other [1]. The shapes and sizes of these voids can be very varied. Based on the behavior of the liquid inside the porous medium, it is possible to distinguish three main groups of voids [2]. In the smaller voids, called molecular pores, the intermolecular forces between the walls and a liquid are very high, while in the largest voids, the movement of the liquid is partially determined by its interaction with the solid part. This type of void is referred to as a cavern. Finally, voids that occupy an intermediate position between the two first types of void are known simply as pores. Fluid flow in a porous medium is only possible when at least one part of each pore communicates with another. Connected pores represent an active porous space, while all the pores in the medium constitute the total porous space. The most important parameters characterizing porous media are the porosity ($\varepsilon$) and the

permeability ($\phi$): the porosity is defined as the ratio between the void volume and the total volume of the medium [3], while the permeability characterizes the capability of a porous medium to conduct a fluid through it under a given pressure gradient.

Ex-poro-hydrodynamic (XPHD) lubrication is a biomimetic-inspired lubrication mechanism, defined by Pascovici in 2001 [4], that consists of self-sustaining fluid films generated in highly compressible porous layers imbibed with liquids, whose solid phase induces compressive elastic forces that are negligible compared to the hydrodynamic forces generated within the porous medium. The principle of XPHD lubrication for tangential movement is shown schematically in Figure 1: the displacement of a dislocator (solid part with discontinuous geometry) causes flow inside the porous media. It should be noted that this type of lubrication is highly dependent on the variation in porosity, and therefore on the variation in the permeability of the porous media.

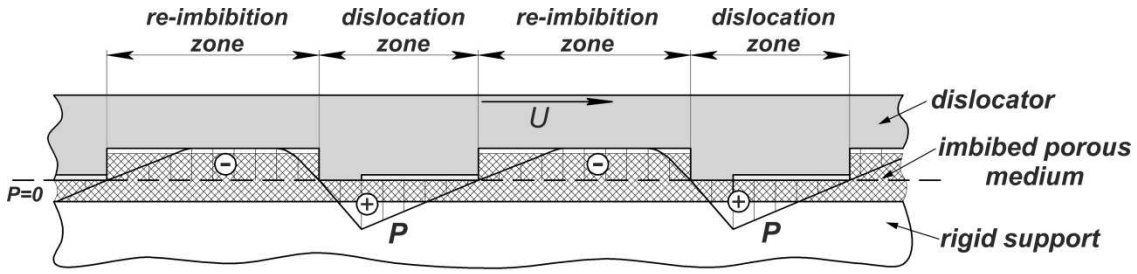


***Figure 1: Principle of XPHD lubrication***

The essential idea of XPHD lubrication is to replace the antifriction material and the thin fluid film, traditionally used in classical sliding motion, with a porous layer imbibed with a fluid that provides a higher load carrying capacity. This type of lubrication represents a completely new technological solution that breaks with current practices and can replace petroleum lubricants, creating self-lubricating and therefore more ecologically sustainable and less expensive tribological systems.

Prof. M.D. Pascovici and his team can be considered the pioneers of XPHD lubrication. In 1994, Pascovici patented a device for pumping a liquid via the dislocation effect [5]. This invention was a viscous pump consisting of a Rayleigh step dislocator and a smooth surface with a porous elastic layer imbibed with a liquid (Figure 2). The dislocator displaces the liquid absorbed by the porous material and propels it along the pipe through a hole in the maximum pressure zone. Experimental results showed a significant increase in fluid velocity and consequently in flow rate compared to the conventional configuration (without a porous layer).

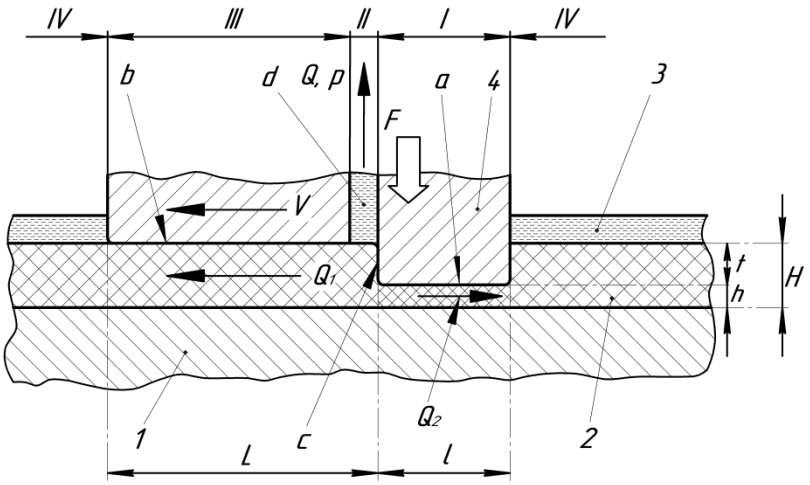


***Figure 2: Scheme patented by Pascovici: procedure and device for pumping via fluid dislocation [5] (I** – deformation zone of elastic layer**; II** – fluid collection zone**; III** – sealing zone to reduce fluid leakage in relative movement direction**; IV** – imbibition zone**; 1** – stationary surface**; 2** – compliant porous media**; 3** – lubricant**; 4** – dislocator**; a, b** – plain surfaces**; c** – step**; d** – fluid acceptor**; Q** – flow rate**; p** – flow pressure**; F** – applied load**; V** – relative speed**; $Q_1$, $Q_2$** – flow rate for each dislocation zone**; H** – thickness of non-deformed porous layer, imbibed with lubricant**; h** – thickness of deformed porous layer**; t** – dislocator step height**; L, l** – length of each dislocation zone**)***

Later, Pascovici designed a test rig [4] that was mainly intended to explore the XPHD effect in the context of tangential movement, and in particular applications involving thrust bearings. In this case, a thrust bearing consists of a fixed dislocator in a Rayleigh configuration and a moving thrust block with a layer of imbibed porous material. Tests were carried out using two liquids (water and oil) in combination with different porous materials (felt and cotton+cellulose). The first tests proved that the pressure generated by the XPHD effect was greater than that obtained in the case of the hydrodynamic regime. The experimental results demonstrated the feasibility of the mechanism of XPHD lubrication, and in particular its performance for low-speed conditions in which other hydrodynamic mechanisms are ineffective. In parallel to this experimental research, Pascovici proposed a simplified analytical model of XPHD lubrication by introducing the following hypotheses:

- The lubricant is Newtonian, and the flow in the porous layers is fully developed and isothermal;
- The flow in the porous medium is described by the Darcy's law;
- The pressure across the porous layer is constant;
- The permeability is correlated with the porosity by a Kozeny-Carman model;
- The volume of the solid structure of the medium is constant during the dislocation process in the normal direction; and
- The dislocator remains in direct contact with the porous medium.

According to the author, the analytical and experimental results showed fairly satisfactory agreement. Complementary to this topic, a wide range of research has been carried out on the

mechanism of squeezing of porous media imbibed with liquids [6], [7]. Research by Pascovici et al. was not limited only to the technical applications of the effects of XPHD lubrication: they also tackled scientific problems related to macro- and nanotribology. In 2007, Pascovici developed a heuristic model of the lubrication of erythrocytes in narrow capillaries [8], which predicts the movement of erythrocytes in plasma flow. This flux occurs in the endothelial glycocalyx, a porous structure consisting of glycoproteins and proteoglycans. Despite the simplifications applied, the results were very close to those of more complex models.

In the United States, Prof. S. Weinbaum and his co-workers from the City University of New York have extensively studied similar lift effects, with particular emphasis on sliding motion over highly porous and soft materials filled with air. Their model was based on the Darcy-Brinkman equation for flow in porous media. It is worth mentioning one of the main conclusions of these studies: "the lift forces generated can be four or more orders of magnitude greater than classical lubrication theory would predict". This concept has been successfully validated in applications at very different scales, such as the motion of red blood cells in capillaries [9], skiing on fresh powder snow [10], [11], [12] and a novel train track [13], [14], [15].

The team of Prof. G. McKinley at the Massachusetts Institute of Technology have been studying shock absorption by composite plates imbibed with liquids [16], [17], [18]. From a theoretical point of view, they used the Darcy equation to model the flow through the porous layer and made the questionable assumption of constant permeability. However, they presented the first study of a non-Newtonian fluid flow. Experimentally, it was shown that the replacement of high-density polyurethane foam with another low-density glycerine-impregnated protective material for motorcycle helmets gives increased protection with reduced weight.

Very recently, another team from the United States presented both experimental [19, 20] and theoretical studies [21, 22] to demonstrate the significant potential of applying soft porous media for soft lubrication with minimal frictional losses. These authors studied a plane surface gliding over a soft porous structure filled with air, and used the model proposed by Prof. S. Weinbaum's team [10] to predict the pressure generation.

Overall, a literature survey shows that this type of lubrication mechanism can provide several orders of magnitude more damping and load capacity than conventional fluid support elements. However, state of the art research on this topic also shows that there are no real XPDH devices, such as bearings or squeeze film dampers, that can be used in industrial application.

The ultimate aim is to offer innovative XPHD technical solutions that break with current practices and provide efficient support systems in terms of load capacity, friction and reliability. The main

challenge is to find an optimal new material, defined as a complex/composite material formed from a solid porous structure and an imbibed fluid.

The present study investigates the possibility of using open-pore polyurethane foams saturated with water or oil as a candidate porous medium. This porous media is first characterized in terms of its porosity and permeability, and an experimental study is then carried out using a simple thrust bearing test rig. A theoretical model based on the Darcy-Brinkman equation is finally used to predict the experimental results.

## 2. Characterization of the porous medium

Generally, polyurethane foam consists of two phases: a solid phase formed from the polyurethane itself, and a phase that can be represented by a liquid, a gas or a mixture of both. This type of foam is a relatively common and widely available material, and is also inexpensive. It should be noted that this choice does not present the ideal porous material for our application, but makes it straightforward to perform theoretical and experimental studies, and to evaluate the performance of XPHD lubrication.

Our characterization of the foam began with simple observation under a microscope, with the objective of understanding the internal structure of the foam, in order to obtain initial qualitative information on the size and shape of the pores.

Figure 3 shows photographs of the macroscopic structure of the foam observed under 20x magnification microscopes (the fine grid in the background is derived from the image of a calibration pattern used to obtain the pore sizes). These observations show that some facets of the cells contain polyurethane residues that appeared after the chemical reactions during the production of the foam. These residues are in the form of protuberances or fine wires and, in some instances, of membranes. This can lead to partially or wholly closed pores, which are able to disturb or block the flow inside the foam. It can be surmised that these residues may have some influence on the porosity and thus on the permeability of the foam.

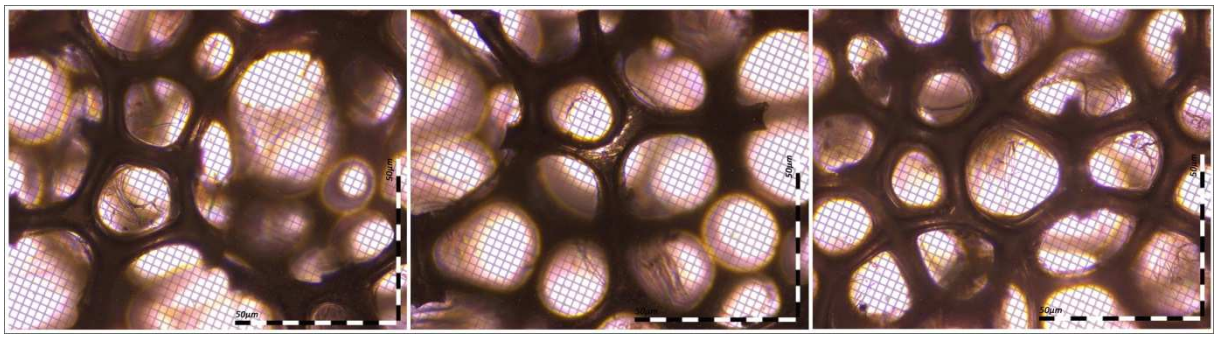

***Figure 3: Foam under 20x magnification***

### 2.1. Measurement of the porosity

The porosity measurements consisted of finding the ratio between the pore volume ($V_p$) and the total volume ($V_t$) of a foam sample. To measure the porosity of polyurethane foam, two methods were used: the weight method and X-ray computed tomography. The use of two different methods makes it possible to obtain more reliable values of porosity; the second method also makes it possible to measure the porosity for different thicknesses of foam and to carry out a numerical reconstruction of the porous structure.

The weight method is based on the capability of the porous material to absorb a liquid (water in our case). The following procedure was applied to perform these measurements (as an aid to understanding, the different steps are illustrated schematically in Figure 4):

1. Five cylindrical samples of the same size were randomly cut from an initial board using a hollow punch. The samples were characterized by two geometric dimensions: the diameter (*D*) and the thickness or height (*h*). The apparent volume of the sample was calculated by the following relation:

$$V_{apparent} = \frac{\pi D^2}{4} h \quad (1)$$

The dry mass ($m_{dry\ specimen}$) of each sample was measured before being attached to a steel wire.

2. The mass of an empty beaker ($m_{beaker}$) and the mass of a spatula ($m_{spatula}$) were also measured.
3. The beaker was filled with water, and the initial mass of water ($m_{H_2O\ initial}$) was determined by deducting the mass of the beaker.
4. In the next step, the sample was immersed in the beaker with water. To ensure maximum imbibition of the foam, it was compressed with a spatula and left in water for five minutes.
5. The impregnated sample was removed from the beaker (leaving the spatula in the beaker) and the mass of water ($m_{H_2O}$) in the beaker was measured again by deducting the mass of the spatula. Using a simple expression ($m_{H_2O\ initial} - m_{H_2O}$) we obtain the mass of water absorbed by the foam ($m_{H_2O\ absorbed}$). Supposing that the volume of absorbed water is equal to the pore volume of the sample, we can obtain:

$$V_{H_2O\ absorbed} = \frac{m_{H_2O\ absorbed}}{\rho_{H_2O}} = V_{pores} \quad (2)$$

6. Finally, the porosity of the sample (i.e. the non-compressed foam) was determined by:

$$\varepsilon_0 = \frac{V_{pores}}{V_{apparent}} \quad (3)$$

7. To determine the porosity of the foam for different compression ratios $\varepsilon_{compr}$, the following analytical expression was used:

$$(1-\varepsilon_{compr})h_{compr} = (1-\varepsilon_0)h_0 \quad (4)$$

where $h_{compr}$ is the thickness of the compressed layer.

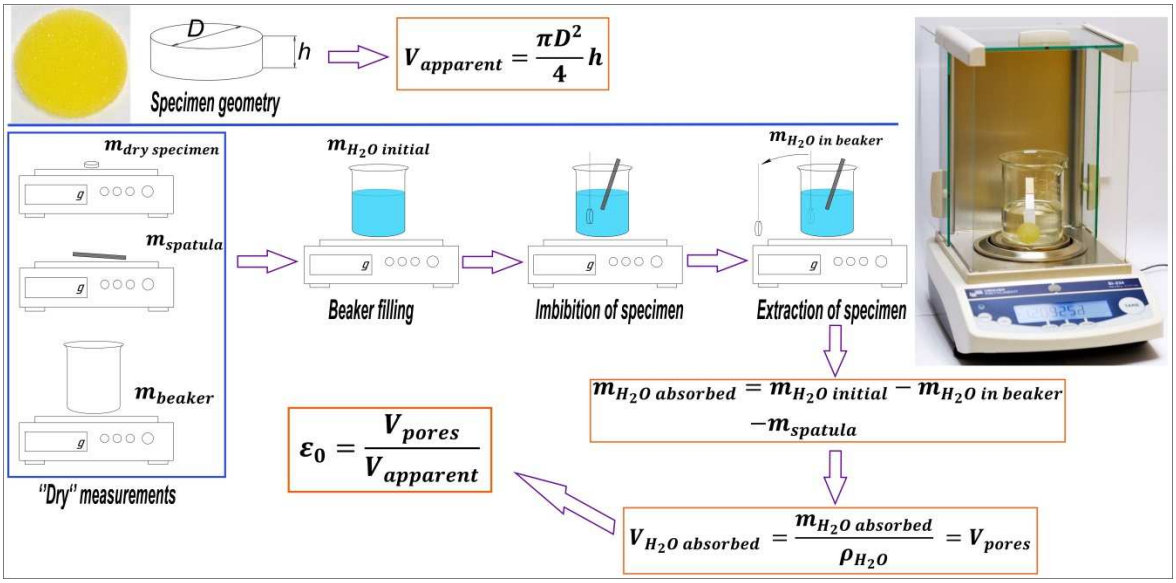


***Figure 4: Measurement of the porosity by the weight method***

A summary of the measurements of porosity using the weight method with water is given in Table 1. The mean value is 0.947 with a standard deviation of 0.043.

| *№ of sample* | *Porosity* |
|---|---|
| 1 | 0.931 |
| 2 | 0.957 |
| 3 | 0.988 |
| 4 | 0.978 |
| 5 | 0.880 |
| ***Average*** | **0.947** |

***Table 1: Summary of porosity measurements using the weight method***

It can be seen in Table 1 that the results obtained with the weight method show an important dispersion. As expected, the accuracy of this method can be influenced by several factors: the initial geometry of the samples which can be slightly different, the presence or not of closed pores, the sample soaking which can be more or less well done, the handling of the samples especially during step 4 described above.

The second method for measuring porosity was based on a multidirectional analysis of the interaction of an X-ray beam with the studied material. X-ray tomography not only allows access to the interior of the material, but also allows for very fine location of all the singularities, heterogeneities and voids that are present within it. To perform these porosity measurements, an ultra high performance tomography system was used (a general view of this system is shown in Figure 5). This tomograph allowed for measurements with a precision grid of 5.74 µm.

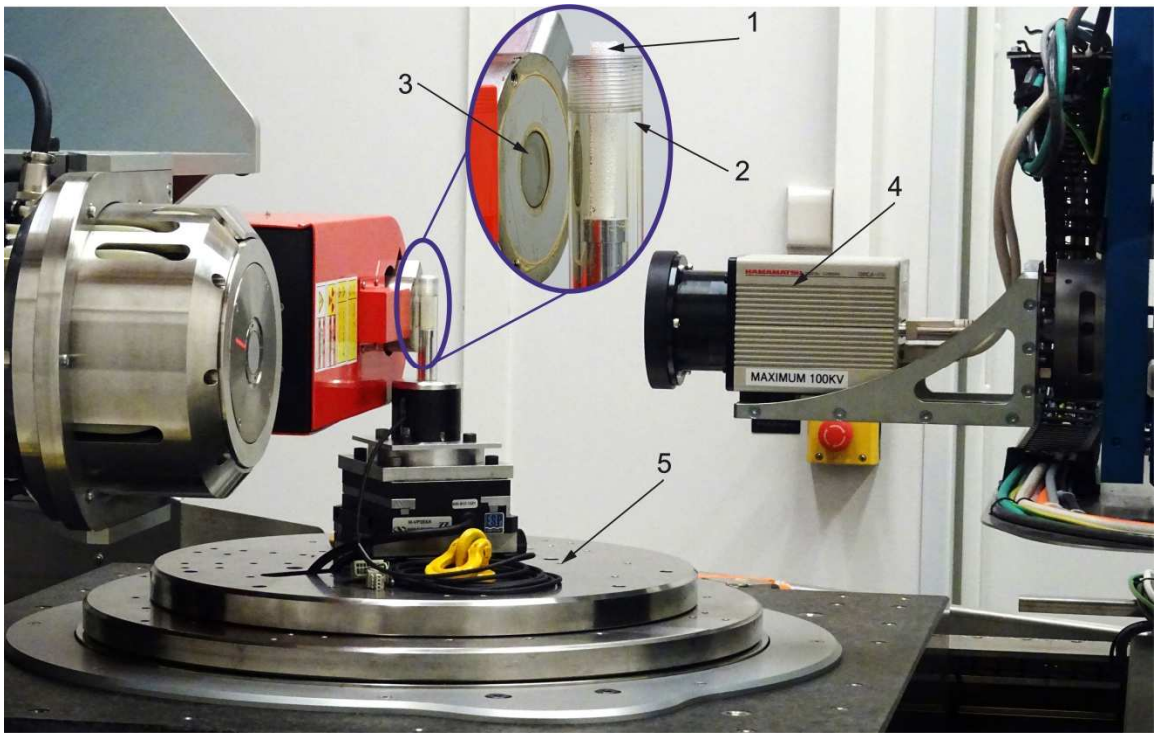


***Figure 5: Ultra high performance X-ray tomography system [1 – specimen, 2 – transparent tube, 3 – X-ray generator, 4 – imager, 5 – air bearing rotation stage and motion axes]***

Before the measurements were taken, a rectangular-shaped foam sample was inserted in a Plexiglas tube holder. The tube was then positioned next to the X-ray generator. On the opposite side, a CCD sensor with very high sensitivity and resolution was used. The X-ray source and the CCD sensor were fixed, while the tube including the sample was mounted on a horizontal plate allowing rotation in the field around the vertical axis. The X-ray beam was passed through the sample and picked up by the imager, which generated analogue signals in proportion to the number of photons received.

The scanning was carried out layer by layer, with a predefined step. The data acquired during the measurements were collected in multiple orientations, and then correlated with each other to ensure the most accurate reconstruction of the studied sample. Using these data, digital images were calculated and reconstructed in grayscale. Each level of gray is used to express, point by point, the local attenuation coefficient of the incident X-ray beam, corresponding in practice to a density scale.

The results of these microtomographic measurements were represented by a sequence of 1339 raw images. To be able to study these images, they needed to be processed using specific software (Figure 6).

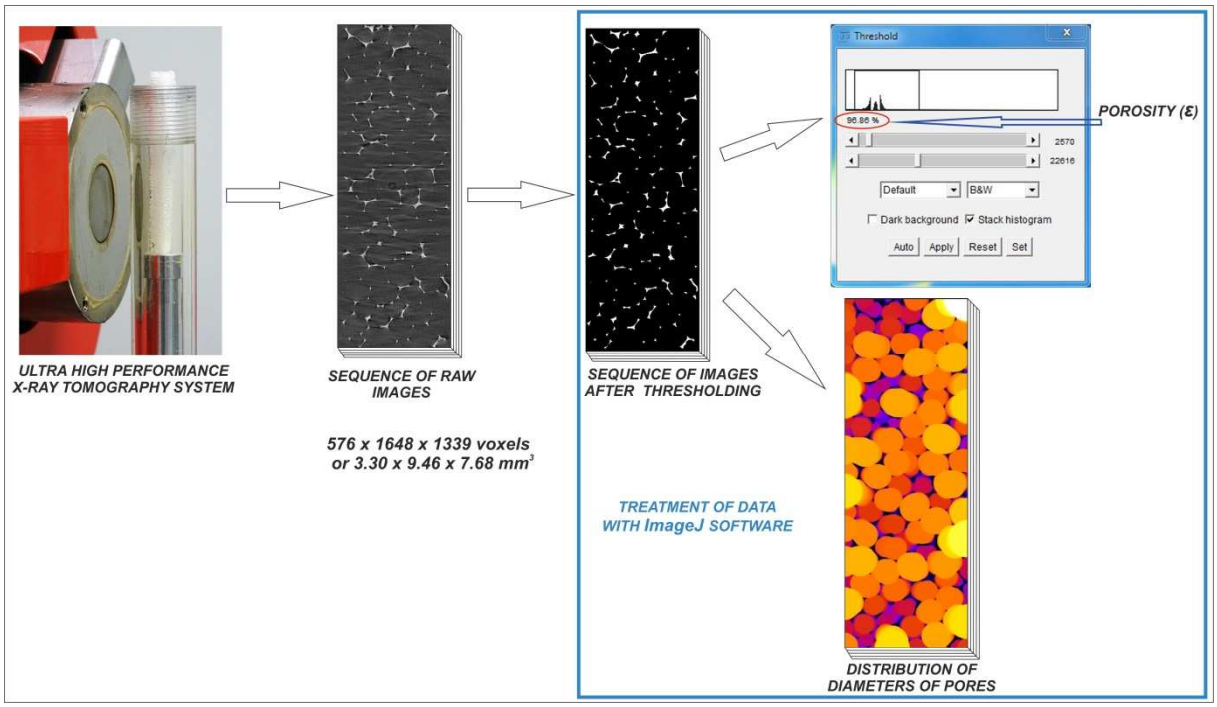


***Figure 6: Processing of raw images with ImageJ software***

In the next step, thresholding of the image sequences was performed. The images were binarized: the initial images encoded using 255 gray levels were transformed into images containing only black and white pixels. This thresholding allowed us to obtain clear images of the studied sample (i.e. without artifacts or parasitic noise) and to establish the percentage of black (empty) and white (matter) pixels for all images representing the sample, thus directly giving the porosity of the foam. A three-dimensional reconstruction of the sample was performed using the same binarized images, and the results are shown in Figure 7.

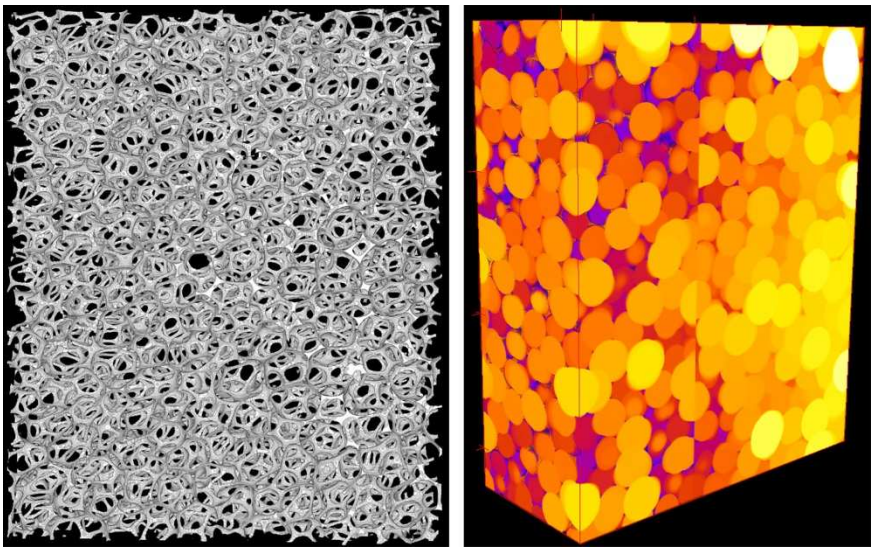

***Figure 7: Three-dimensional reconstruction (left) and determination of the average diameter of the pores (right)***

The average diameter of the pores was determined using the same binarized image sequence as used during the reconstruction operation. By replacing the black areas representing the pores with spheres of varying diameters, we obtained a new sequence of images with circles of different colors (Figure 7), in which each color corresponded to an average sphere diameter. The reconstruction of this sequence of images formed a volume filled with spheres, where the volume of the voids between the spheres represented the volume occupied by the material of the foam. This new sequence of images was analyzed to extract a histogram giving the populations of spheres of the same color (in fact, the histogram gave the number of pixels assigned to each color within the volume under consideration). Based on the diameters of the spheres and the number of associated pixels corresponding to each color (Figure 8a), we could determine the number of spheres of the same diameter contained in the volume (Figure 8b). By recalculating the volume of a sphere of each color, it was possible to find the average diameter of the pores as well as a quantitative representation.

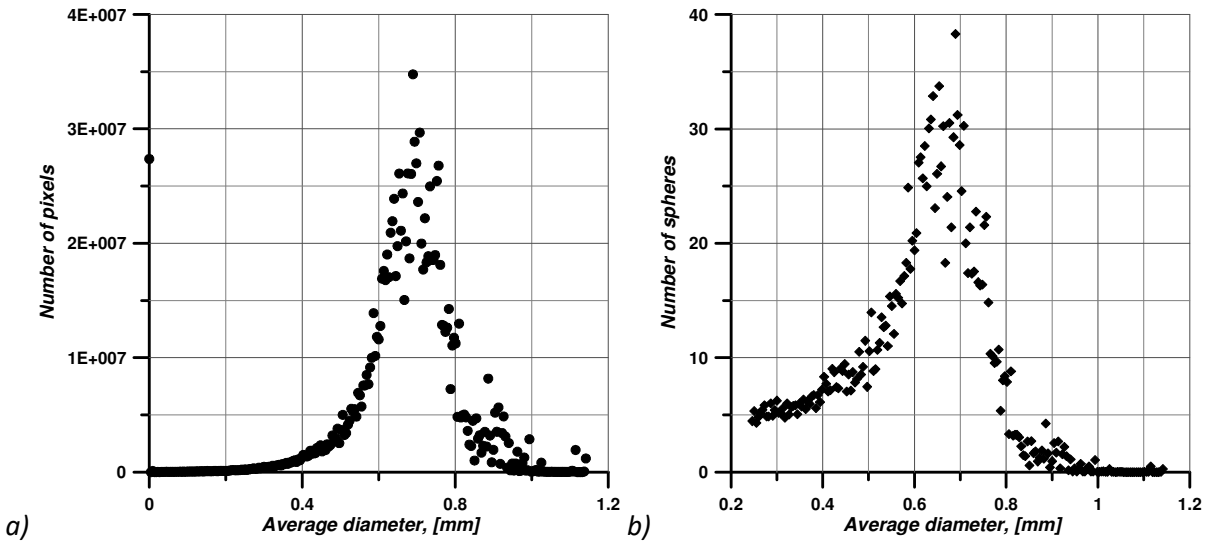


***Figure 8: Pore distribution in foam sample***

This three-dimensional reconstruction of foam and analysis of the pore distribution allowed us to confirm the variation in pore sizes observed under the microscope. The results of these measurements showed that the pore distribution was approximately Gaussian, with a standard deviation $\sigma = 0.260$ mm. The pore diameters ranged from 0.246 to 1.141 mm, and the average diameter was 0.667 mm.

The results of porosity measurements using both methods are shown in Table 2. The slight difference between the values for the porosity can be explained by the presence of air inside the foam. Despite the pre-imbibition of the foam, a certain amount of air still remained trapped within the sample and had a negative impact on the precision of the weight method. For this reason, the value of the porosity measured using X-ray tomography seemed more credible, and was therefore selected for the subsequent study.

| ***Porosity by weight method*** | ***Porosity by tomography*** | ***Error, %*** |
|---|---|---|
| ***0.947*** | ***0.960*** | ***1.35*** |

***Table 2: Summary of porosity measurements***

### 2.2. Measurement of permeability

The principle of permeability measurement consists of measuring the flow rate of a liquid of a given viscosity through a sample under a pressure gradient that causes a flow. The schema of the in-plane permeameter used for this study, inspired by the work of Lundström et al. [23], is presented in Figure 9. The experimental device consisted of an aluminium bedplate (12) with a rectangular section channel machined in its upper part. Four adjustable legs (13) allowed a horizontal position to be ensured for the permeameter. Variation in the pressure was applied using a pressure regulator (5). To control the pressure variation, the permeameter was instrumented with a manometer (3) and a

pressure sensor (4) connected to a computer. A drain valve (2) was installed in front of the pressure sensor to allow the air to be purged, therefore avoiding disturbance of the measured inlet pressure. A pressure compensation pocket (9) was machined around the inlet and provided a uniform pressure field in front of the foam sample.

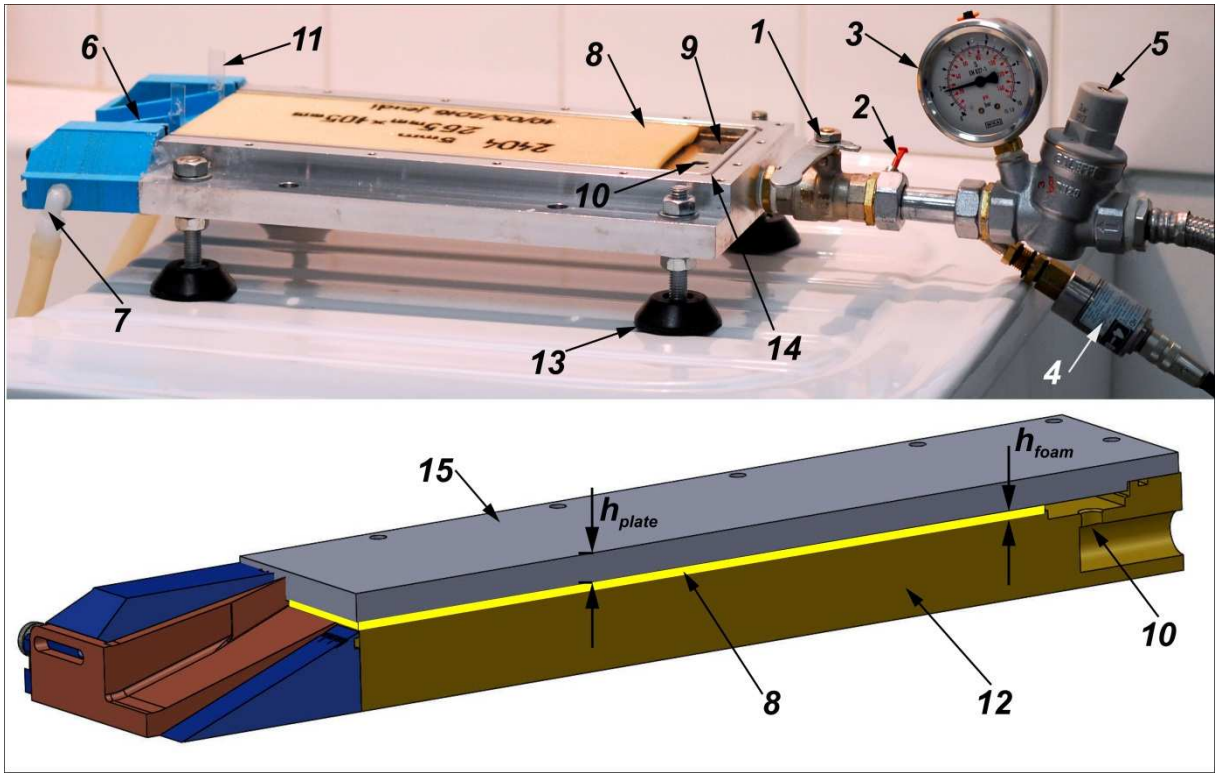


***Figure 9: Longitudinal permeameter: 1 – valve, 2 – drain valve; 3 – manometer, 4 – pressure sensor, 5 – pressure regulator, 6 – adjustable funnel, 7 – lateral flow evacuation, 8 – foam, 9 – pressure compensation pocket, 10 – fluid acceptor, 11 – supplementary deflector, 12 – bedplate, 13 – adjustable legs, 14 – rectangular groove, 15 – top shape plate***

The permeameter allowed measurements to be made for different foam compression rates. This was achieved by an assortment of top-shaped plates (15) of different thicknesses. An additional set of plexiglass plates allowed the flow through the foam sample to be visualized. The assembled permeameter was sealed with an O-ring inserted in a rectangular groove machined on the edge of the plate. As suggested in [23], evacuation of the fluid occurred via an adjustable funnel (6) which allowed for a variable width of the exhaust duct and thus separation of the lateral flow from the main flow used to determine the permeability.

The procedure for preparing the permeameter for a test campaign comprised three main steps: cutting the foam, fixing the sample inside the permeameter and the final assembly of the permeameter. The sample was fixed with double-sided tape reinforced with high-strength fiberglass, with a permanent adhesive that had a high resistance in contact with fluids. The entire surface between the underside of the sample and the bedplate was fixed. However, it should be noted that

the adhesive tape had an average thickness of about 0.22 mm, thus slightly modifying the compression ratio of the foam sample. In the following calculation of permeability, this value is deducted to give the correct compression ratio of the foam.

An optimal sample size of 265 x 105 mm (i.e. slightly wider than the rectangular channel size of 260 x 100 mm) was chosen after verification tests, creating a compacted layer at the edges and thus reducing the influence of the edge effect. In addition, the funnel was adjusted to a value of 60 mm in order to recover sufficient fluid and to avoid effects from the lateral flow.

Once the permeameter was assembled and prepared, the fluid (water at a pressure of 0.1 MPa) was allowed to flow through the sample for 30 minutes for each foam compression ratio. This step was necessary to fully remove air from the foam. Measurements for each compression ratio were made for pressure values of 0.07, 0.1, 0.12, 0.15, 0.2, 0.25 and 0.3 MPa. To achieve a stable flow rate after each pressure change, a pressure stabilization time of 10 minutes was used.

The test campaign consisted of three consecutive series of measurements, each of which included seven flow rate measurements for each supply pressure. It should be noted that the amount of fluid passing through the sample was measured over a pre-established time interval, whereas the flow rate and the permeability were calculated.

The raw experimental results presented in Figure 10 show the variation in the flow rate as a function of the supply pressure.

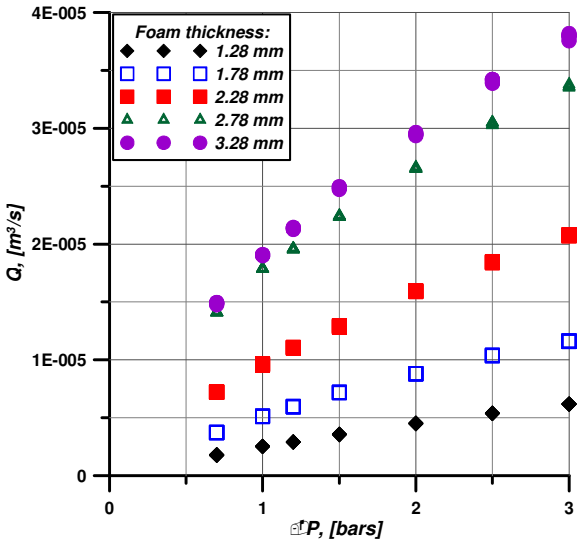


***Figure 10: Raw results of permeability measurements***

In order to interpret the experimental results and thus determine the permeability of the foam, it was necessary to create a model to describe the flow in the porous medium. A first attempt to assess the permeability $\phi$ of the foam was made with the classic Darcy model:

$$\frac{\partial p}{\partial x} = \frac{\Delta P}{L} = -\frac{\mu}{\phi} u \quad (5)$$

where $L$ is the length of the tested sample, $\mu$ the fluid viscosity and $u$ the fluid velocity obtained by dividing the flow rate by the cross-section area of the sample:

$$u = \frac{Q}{A_e} = \frac{Q}{b*h} \quad (6)$$

where $A_e = b * h$ is the cross-section area of the sample, and $b$ and $h$ are the width and the thickness of the foam, respectively. For a given viscosity, a least-squares linear curve fit for a plot of pressure drop versus fluid velocity was used to give the Darcy permeability.

If the permeability of the medium is constant throughout its thickness, the Darcy model assumes that the velocity of the fluid is also constant. In reality, at the boundaries between the porous layer and the upper and lower walls, the velocity of the fluid goes to zero (reflecting generally accepted non-slip conditions). This induces a variation in fluid velocity with the thickness of the layer, which cannot be predicted with the Darcy model. In view of this, and following the study presented in [24], permeability was also estimated using the Darcy-Brinkman model:

$$\frac{\partial p}{\partial x} = -\frac{\mu}{\phi} u + \mu' \frac{\partial^2 u}{\partial y^2} \quad (7)$$

where $\mu'$ is the so-called effective viscosity and is calculated here as the ratio between the dynamic viscosity and the medium porosity:

$$\mu' = \frac{\mu}{\varepsilon} \quad (8)$$

By integrating Equation (7), the fluid velocity can be written as a function of the thickness of the porous layer:

$$u(y) = C_1 \, sinh(\omega \, y) + C_2 \, cosh(\omega y) - \frac{\phi}{\mu} \frac{\partial p}{\partial x} \quad (9)$$

where $C_1$ and $C_2$ are two integration constants and $\omega = \sqrt{\frac{\varepsilon}{\phi}}$. Applying the non-slip boundary conditions, Equation (9) takes the following form:

$$u(y) = \frac{\phi}{\mu} \frac{\partial p}{\partial x} \left( \frac{1 - cosh(\omega h)}{sinh(\omega h)} sinh(\omega y) + cosh(\omega y) - 1 \right) \quad (10)$$

The integration of the fluid velocity through the thickness of the porous layer gives the volumetric flow rate:

$$Q(\phi) = b \int_0^h u(y) dy = -b \frac{\phi}{\mu} \frac{\partial p}{\partial x} \left( h - 2 \frac{1 - \cosh(\omega h)}{\omega \sinh(\omega h)} \right) \quad (11)$$

Once again, a least-squares curve fit to the rate of flow versus the pressure difference is used to give the Darcy-Brinkman permeability.

Figure 11a compares the Darcy and the Darcy-Brinkman permeabilities, represented as a function of porosity. It can be seen that the differences are small, leading to the conclusion that for the foams studied here, the Darcy-Brinkman model does not cause any significant changes in the estimated permeability. The influence of the Brinkman extension is illustrated in Figure 11b, which shows the variation in the fluid velocity with the thickness of the sample: here, we present the results for a compressed foam thickness of 3.28 mm (i.e. ε=0.939), although other measurements lead to similar trends. As can be seen from the figure, the differences between the two models are limited to a very thin layer near the boundaries between the walls and the porous medium, where the Darcy-Brinkman model meets the non-slip boundary conditions (area surrounded by orange dotted lines).

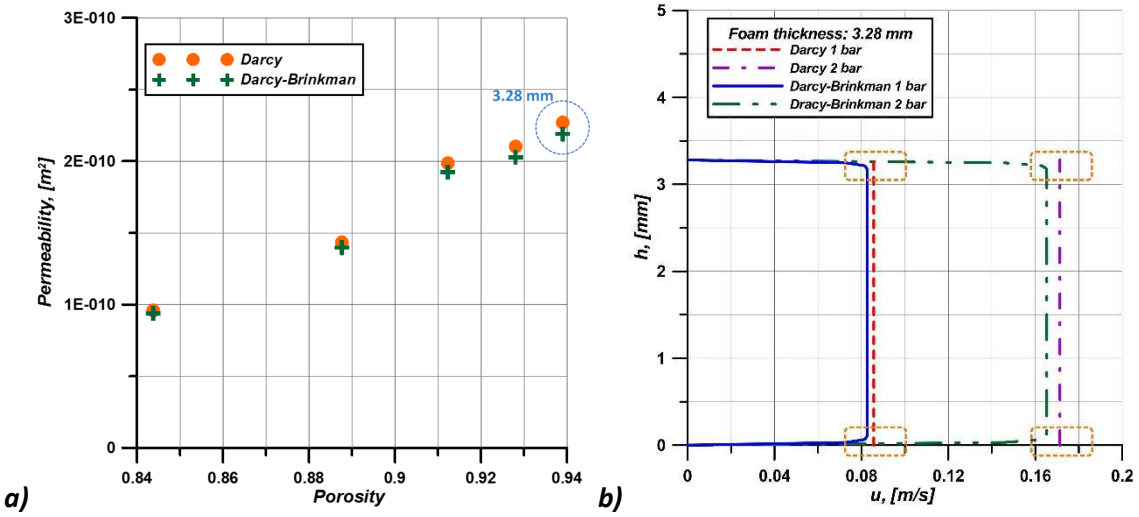


***Figure 11: Results for Darcy and Darcy-Brinkman models: a) variation in permeability as a function of porosity, b) velocity profile for Darcy and Darcy-Brinkman models at ε=0.939 (h=3.28 mm)***

Both Darcy and Darcy-Brinkman interpretations of the experimental results assume that the variation in the volumetric rate of flow is linear with the pressure gradient. As shown in Figure 10, for a high foam thickness (i.e. higher porosity), the flow rate deviates from a straight line. A complementary analysis was therefore carried out by including in the interpretation of the results the so-called Dupuit-Forchheimer correction, which accounts for drag forces [25]. In order to simplify the calculations, and based on the fact that the Brinkman model does not introduce significant corrections, it is assumed that the flow can be correctly described by the following equation:

$$\frac{\partial p}{\partial x} = \frac{\Delta P}{L} = -\frac{\mu}{\phi}u + \frac{C_f \rho}{\sqrt{\phi}}|u|u \qquad (12)$$

where $C_f$ is a constant that varies with the porosity of the medium. Equation 12 assumes that the variation in the pressure gradient with the velocity of the fluid is parabolic. The method proposed by Boomsma and Poulikakos [26] was used to determine the Darcy-Forchheimer permeability. By introducing the coefficients $A_{DF} = \frac{\mu}{\phi}$ and $B_{DF} = \frac{C_f \rho}{\sqrt{\phi}}$, Equation (12) becomes:

$$\frac{\Delta P}{L} = -A_{DF}u + B_{DF}u^2 \tag{13}$$

where the coefficients $A_{DF}$ and $B_{DF}$ can be determined by the least-squares method:

$$A_{DF} = \frac{\left(\frac{1}{L}\sum_{i=1}^{n} u_i \Delta P_i\right)\left(\sum_{i=1}^{n} u_i^4\right) - \left(\frac{1}{L}\sum_{i=1}^{n} u_i^2 \Delta P_i\right)\left(\sum_{i=1}^{n} u_i^3\right)}{\left(\sum_{i=1}^{n} u_i^2\right)\left(\sum_{i=1}^{n} u_i^4\right) - \left(\sum_{i=1}^{n} u_i^3\right)\left(\sum_{i=1}^{n} u_i^3\right)} \tag{14}$$

$$B_{DF} = \frac{\left(\frac{1}{L}\sum_{i=1}^{n} u_i^2 \Delta P_i\right)\left(\sum_{i=1}^{n} u_i^2\right) - \left(\frac{1}{L}\sum_{i=1}^{n} u_i \Delta P_i\right)\left(\sum_{i=1}^{n} u_i^3\right)}{\left(\sum_{i=1}^{n} u_i^2\right)\left(\sum_{i=1}^{n} u_i^4\right) - \left(\sum_{i=1}^{n} u_i^3\right)\left(\sum_{i=1}^{n} u_i^3\right)} \tag{15}$$

a)

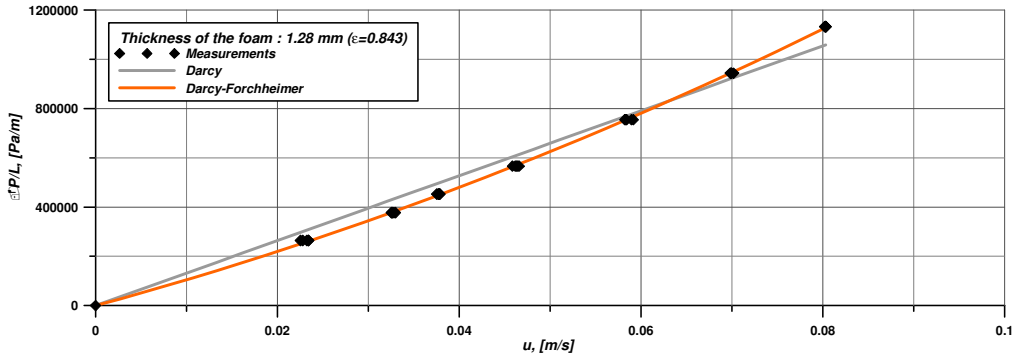


b)

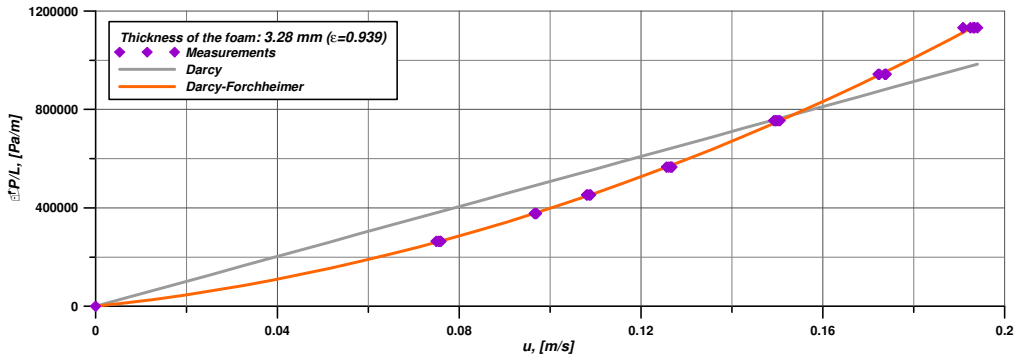


***Figure 12: Interpretation of results of water permeability measurements***

Figure 12 compares the Darcy and Darcy-Forchheimer approximations of the variation in the pressure gradient relative to the mean fluid velocity. The results are presented for both a high (Figure 12 a) and a low compression rate (Figure 12 b). It is clear that the correlation with the experimental results is better with the Darcy-Forchheimer model.

The comparison between the permeabilities obtained by the three models is shown in Figure 13a. It can be observed that the difference between the calculated values increases with increasing porosity. At the same time, it can be seen that the Forchheimer's coefficient is not a constant coefficient, but varies with the porosity (i.e. with the compression ratio) of the foam (Figure 13b). On the basis of the so-called Ergun equation, some authors have considered that $C_f$ can be written as the ratio between a form-drag material constant $C$ and $\sqrt{\varepsilon^3}$ : $C_f = \frac{C}{\sqrt{\varepsilon^3}}$ [3]. The solid line in Figure 13b) represents the least-squares approximation of the experimental variation, which leads to $C$ = 0.46. The Forchheimer's coefficient decreases with increasing porosity but a marked discontinuity in $C_f$

experimental values between the porosity values 0.91 and 0.93 can be noted. No real explanation for this behavior can be given and future investigations will be necessary.

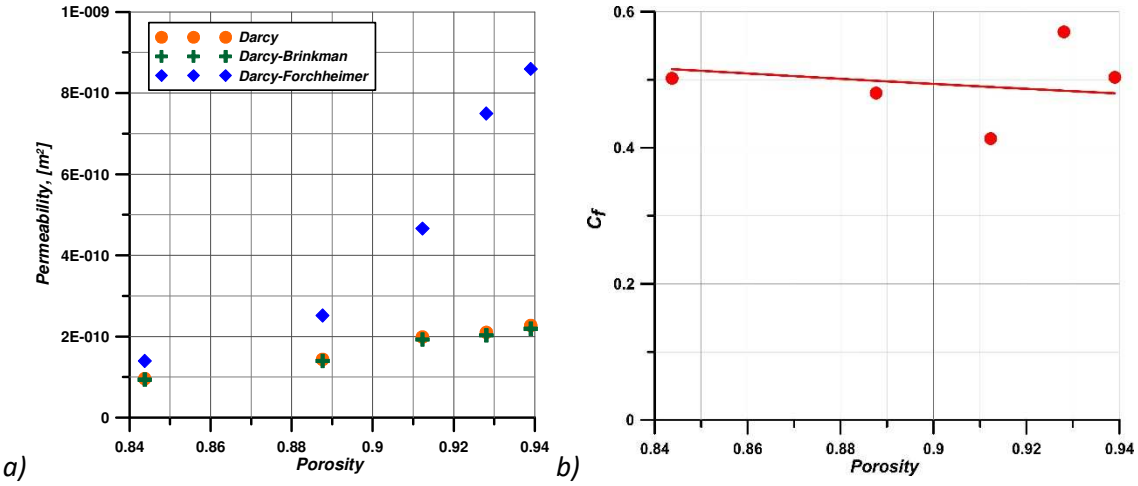


***Figure 13: Measurement results: a) permeabilities determined by three models; b) variation in the Forchheimer coefficient as a function of porosity.***

### 2.3. Uniaxial compression tests

Uniaxial compression tests were carried out on foam samples with a diameter of 80 mm and a thickness of 5 mm (the same dimensions as the samples used in the experimental tests described below). The measurement procedure was based on ISO 3386-1:1986 [27], which specifies a method for the determination of the relative stress-strain characteristics in compression for low-density polymeric foam materials of up to 250 kg/m$^3$. This standard specifies that the foam sample inserted between two flat surfaces must be compressed three consecutive times by up to 40% of its initial thickness; the fourth compression is used as a reference test to determine the behavior of the foam under compression. The test results for dry and soaked new foams are shown in Figure 14. The graphs in this figure include two phases: the compression phase and the decompression phase of the sample. By analyzing these graphs, we can see the phenomenon of hysteresis, as the area between two curves (compression and decompression) corresponds to the energy dissipated by the foam; in the decompression phase, the stresses are gradually reduced. It is also noted that the fluid has a significant impact on the behavior of the foam. We can see that the presence of water significantly reduces the stress, and that the hysteresis phenomenon is less marked.

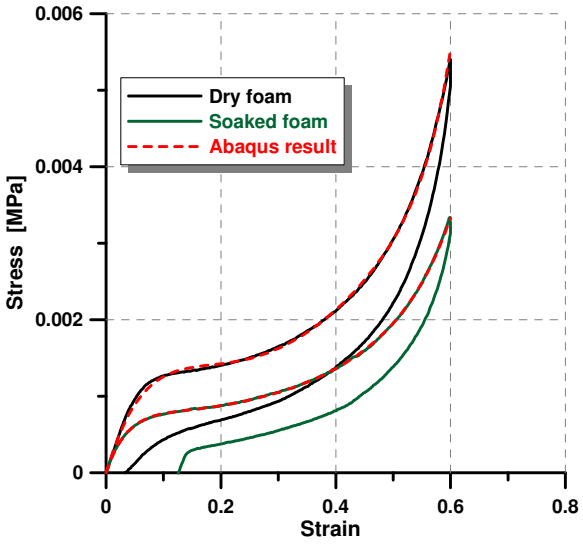


***Figure 14: Stress vs. strain for uniaxial compression tests***

In order to model the behavior of the foam, a compression test was simulated using Abaqus software. The experimental stress-strain data obtained during the experimental compression of the foam were entered directly into the calculation software to find the most suitable behavior law. The response of the material is defined by the parameters of a strain energy function [28]. As can be seen from Figure 14, a comparison between these simulations and the experimental measurements gave quite good results.

# 3. Experimental results for XPHD thrust bearing

In order to investigate the performance of polyurethane foam as a possible candidate for a new design of XPHD thrust bearing, a specific test bench was developed. A general view is shown in Figure 15a. The XPHD lubrication test bench consisted of a vertical spindle (1) supported by two ball bearings. An electric motor set in motion the spindle from 0 to 250 rpm via a belt drive, and the rotational speed was measured by an inductive sensor placed on the drive pulley. A schematic view of the test cell is given in Figure 15b. The sample of porous material was fixed on the flat surface of the mobile thrust block (3) installed on the spindle nose. The fixed thrust block (5) was connected to the upper guide arm (9) via a torque meter (6) and various intermediate parts, including a guide (7) and an axis (8). To ensure coaxiality between the mobile and fixed thrust blocks, the positions of the upper guide arm (9) and the axis (8) were adjusted. In addition, a ball-and-socket joint with a 13° maximum swivel angle was intended to support the oscillating movements and to compensate for misalignment. The dislocator (4) was attached to the fixed thrust block (5) by means of a central screw and two locking pins. The holes drilled in the fixed thrust block and in the dislocator made it possible to instrument each pad with a thermocouple (11) and a pressure sensor (12) (Figure 15c). The seal between the fixed thrust block and the dislocator at the pressure head area was ensured by

O-rings embedded in special housing. The three thermocouples were fixed, and additional sealing with silicone was applied.

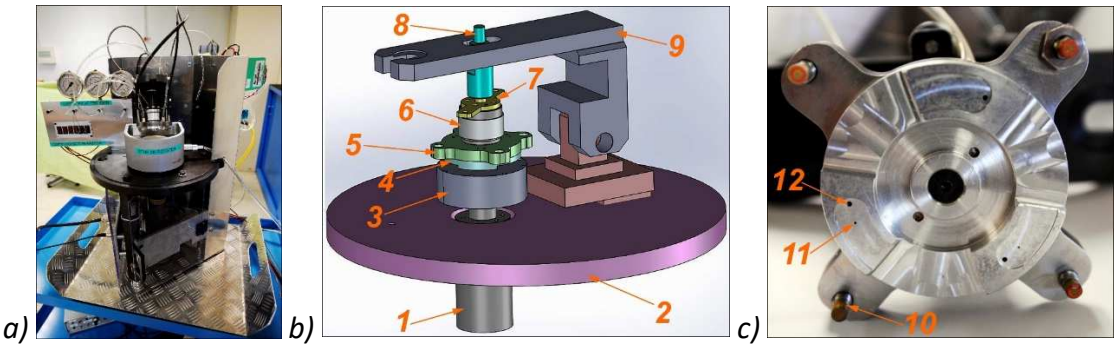


***Figure 15: XPHD lubrication test rig: a) general view, b) experimental cell (view without reservoir and adjustable support), c) fixed thrust block [1 – spindle, 2 – base, 3 – mobile thrust block, 4 – dislocator, 5 – fixed thrust block,6 – torquemeter/intermediate element, 7 – guide, 8 – axis, 9 – upper guide arm, 10 – inductive sensor, 11 – pressure head, 12 – thermocouple]***

The fixed thrust block was equipped with four inductive sensors with a measuring range of up to 1 mm, making it possible to measure the thickness of the film, or more precisely the thickness of the imbibed compressed foam. A contact displacement sensor was also used to control the vertical movement of the fixed thrust block/upper guide arm assembly. However, during the tests, the distance between the mobile thrust block and the dislocator was kept constant. LabVIEW software was used to acquire the signals (rotational speed, temperature, pressure, torque and displacement) and to carry out an initial data analysis.

The dislocator, an essential element of the test rig, came into direct contact with the imbibed foam. The dislocator can have different thrust pad geometries for the same outside diameter, height and number of pads, and in this study, we investigated two different geometries for the dislocator. The first of these, called a pocketed dislocator, consists of three Rayleigh pads with pockets of 0.3 mm depth (Figure 16a). The second, shown in Figure 16b, consists of three inclined plane pads, uniformly distributed around the circumference. The upper surface of each pad is inclined at an angle of 3.70° from the horizontal plane and each pad is equipped with a thermocouple and a pressure head located near the maximum pressure zone.

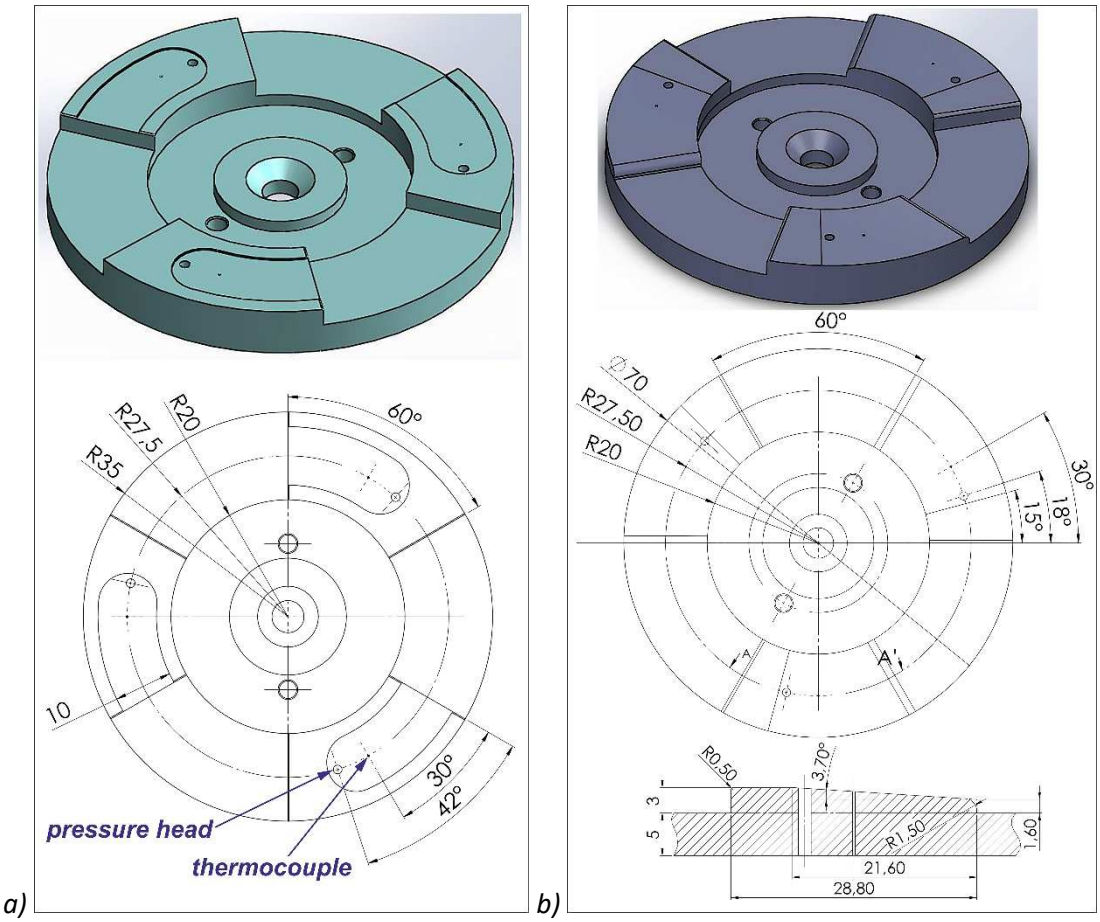


***Figure 16: CAD models of dislocators: a) pocketed dislocator; b) tapered land dislocator***

The following procedure was used for the tests:

- After adjusting the initial gap and fixing a sample of the foam (with thickness 5 mm and diameter 80 mm), the reservoir was filled with the liquid, and the foam sample was imbibed manually with a spatula to improve the penetration of the liquid throughout the sample.
- The tests for each thickness of foam were carried out at rotational speeds ranging from 50 to 250 rpm in steps of 50 rpm.
- After each change of speed, the test rig was allowed to run for 10 seconds to stabilize the pressure generated by the system.
- Experimental data were then recorded for 20 seconds.
- Variations in the thickness of the foam were achieved by the adjustable support, which made it possible to lower or raise the upper guide arm (and hence the dislocator) below or above the initial position.

Three sets of experimental tests were carried out for the pocketed and the tapered land thrust bearing, using water and oil ISO VG 46 (Figure 17). The thickness of the compressed soaked foam ($h_1$) used in these tests varied between 1.2 and 1.7 mm, a range that allowed for variation in the

significant parameters without substantial damage to the sample. In addition, the foam compression rates were similar to the compression rate used for permeability measurements.

The analysis of the experimental results began with the data obtained for the pocketed dislocator. Figure 17a shows the variation in the pressure for three series of tests performed with water. The pressure generated by the XPHD effect increased linearly with the rotational speed, and it can be seen that the pressure tends to decrease from one test to another with the same sample, which can be explained by a change in the mechanical characteristics of the foam. We can assume that the foam became “used up” over a number of tests, and that its mechanical properties in terms of elasticity changed. This was confirmed by uniaxial compression test of the sample that were realized before and after the tests. The maximum pressure measured for the smallest thickness of the foam did not exceed 0.35 bars. Figure 17c shows the pressure variations for the test using the same dislocator in combination with ISO VG 46 oil. Due to the higher viscosity of the oil, the increase observed in the pressure is greater, and with the use of oil, a maximum pressure of about 2.5 bars was reached. However, in the latter case, the pressure variation with the rotational speed is no longer linear, and the rate of increase reduces with the speed. This phenomenon can be explained by problems with the re-imbibition of the foam at higher speeds. The results of experimental tests using the tapered land dislocator are shown in Figure 17b and Figure 17d. It can be noted that the maximum pressure generated by the system with this type of dislocator is higher than for the pocketed dislocator.

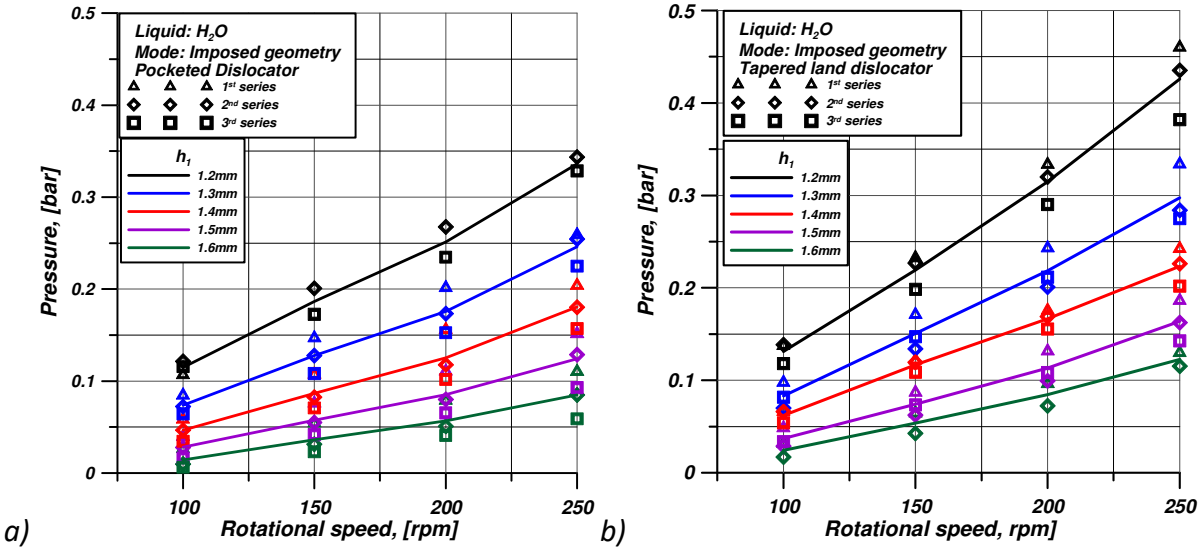

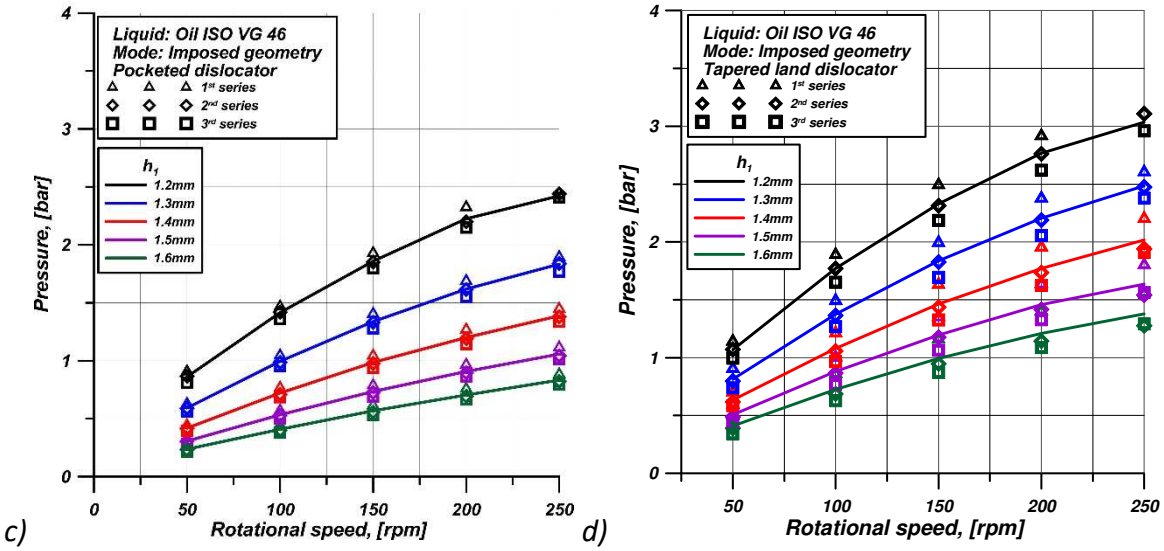


***Figure 17: Pressure variation as a function of rotational speed, obtained with water and ISO VG46 oil [h1=1.2 mm corresponds to ε=0.83]: a) & c) pocketed dislocator; b & d) tapered land dislocator***

The impact of each dislocator type on the structure of the studied sample and thus the wear of the foam for XPHD applications was also investigated. A wear analysis was carried out for foams imbibed with both water and oil ISO VG 46.

For the experimental test with water, a new foam sample was fixed on the mobile thrust block prior to the first series of tests for each type of dislocator. The foam samples were inspected after each test campaign. Photographs of the wear of the foam for both dislocators are shown in Figure 18, and from these, we can see that the wear depends on the geometry of the dislocator, with each dislocator leaving characteristic traces. The pocketed dislocator causes a significant loss of foam material in the area of passage of the pads (in this case, the width of the wear zone corresponds to the width of the pocket - Figure 18a).

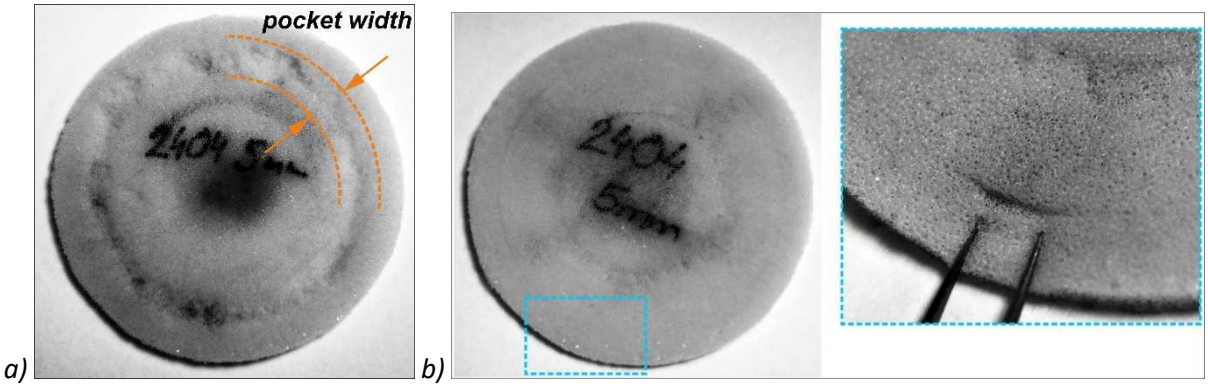


***Figure 18: Foam wear after testing with water and different dislocators: a) pocketed dislocator, b) tapered land dislocator***

The wear of the foam after the test with the tapered land dislocator in combination with water is represented by two circular incisions (Figure 18b), which form a circular ring of width equivalent to

that of the dislocator pad. Despite these circular incisions, the tapered land dislocator does not noticeably destroy the surface of the foam (recall here that this dislocator can generate higher pressure levels than the pocketed dislocator).

For the wear analysis of the foam imbibed with oil, it should be noted that only one sample of foam was used, and this sample underwent three series of tests with each type of dislocator (six series of tests in total) in addition to the endurance tests. This last type of test was carried out over a continuous period of 72 hours with the tapered land dislocator (with the foam sample compressed at 1.3 mm). To avoid thermal exchange between the oil and the ambient air throughout the tests, the test rig was equipped with thermal insulation. Photographs of the foam sample after testing with oil are shown in Figure 19.

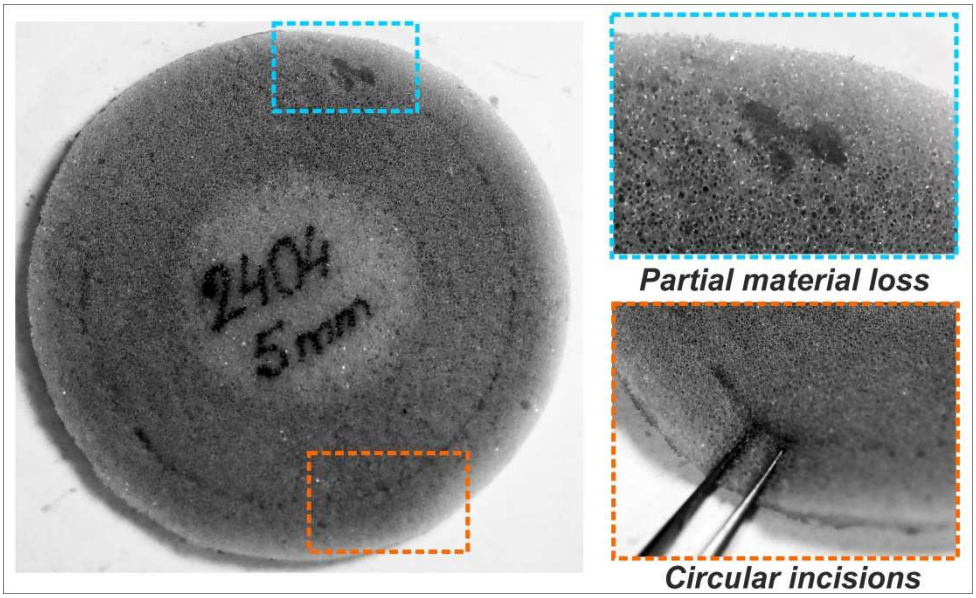


***Figure 19: Foam wear after testing the two types of dislocator with ISO VG 46 oil***

We can observe two types of wear: partial loss of material and circular incisions from the interactions with the pocketed and tapered land dislocators. Despite the significant number of experimental tests carried out using this sample, we can observe that the level of wear of the foam is much less marked with oil than with water. Based on the results of this study, it can be concluded that the lifetime of porous materials in XPHD applications is determined not only by the geometry of dislocator but also by the properties of the lubricants.

# 4. XPHD lubrication model

## 4.1. Mathematical formulation of a Darcy-Brinkman Reynolds-type equation

The XPHD lubrication model is based on a Reynolds-type equation, developed from the Darcy-Brinkman equation and the continuity equation. This model takes into account the main assumptions of lubrication:

- The fluid medium is continuous;
- The fluid experiences a laminar flow;
- The fluid is Newtonian;
- The effects of inertial and gravitational forces are neglected;
- Non-slip boundary conditions are applied between the fluid and contact surface;
- The pressure is constant throughout the thickness of the porous medium.

For a better understanding of the development of our XPHD lubrication model, Figure 20 shows two surfaces corresponding to the dislocator and the rigid support, separated by an imbibed porous material. An orthonormal axis system $(O, \vec{x}, \vec{y}, \vec{z})$ is chosen in which the $\vec{y}$ direction corresponds to the direction following the film thickness. It is also assumed that the flexible porous media exactly follows the geometry of the dislocator, meaning that the deformations in the porous media caused by the geometrical discontinuity of the dislocator are not taken into account.

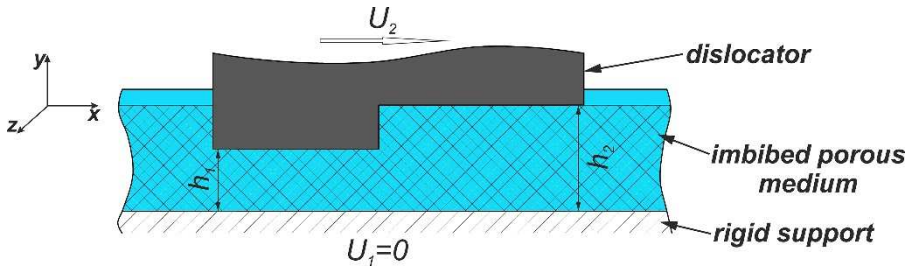


***Figure 20: Axis system and elements of the XPHD system***

For simplicity, the model is presented for the one-dimensional case. Thus, the Darcy-Brinkman equation can be written in the following form:

$$\frac{\partial p}{\partial x} = -\frac{\mu}{\phi}u + \mu' \frac{\partial^2 u}{\partial y^2} \tag{16}$$

where $\mu' = \frac{\mu}{\varepsilon}$ is the effective viscosity. The general solution of the differential equation in (16) can be written as:

$$u(y) = A\, sinh(\omega y) + B\, cosh(\omega y) - \frac{\phi}{\mu}\frac{\partial p}{\partial x} \tag{17}$$

where $\omega = \sqrt{\frac{\mu}{\mu'\phi}} = \sqrt{\frac{\varepsilon}{\phi}}$. The following boundary conditions are used: $u(y = 0) = U_1 = 0$ and $(y = h) = U_2$. Here, $h$ corresponds to the distance between the rigid support and the dislocator. By applying these boundary conditions, the coefficients $A$ and $B$ can be determined:

$$A = \frac{\phi}{\mu}\frac{\partial p}{\partial x}\frac{1}{sinh(\omega h)} - \frac{\phi}{\mu}\frac{\partial p}{\partial x}\frac{cosh(\omega h)}{sinh(\omega h)} + \frac{U_2}{sinh(\omega h)} \;\; ; \;\; B = \frac{\phi}{\mu}\frac{\partial p}{\partial x} \tag{18}$$

and the expression for the velocity therefore becomes:

$$u(y) = \frac{\phi}{\mu}\frac{\partial p}{\partial x}\frac{sinh(\omega y)}{sinh(\omega h)} - \frac{\phi}{\mu}\frac{\partial p}{\partial x}\frac{cosh(\omega h)}{sinh(\omega h)} sinh(\omega y) +$$

$$+U_2\frac{sinh(\omega y)}{sinh(\omega h)}+\frac{\phi}{\mu}\frac{\partial p}{\partial x}cosh(\omega y)-\frac{\phi}{\mu}\frac{\partial p}{\partial x} \quad (19)$$

The mass conservation equation is written as follows:

$$\int_0^h\frac{\partial u}{\partial x}dy+\int_0^h\frac{\partial v}{\partial y}dy=0 \iff \int_0^h\frac{\partial u}{\partial x}dy+V=0 \quad (20)$$

where $V=\frac{dh}{dt}=\frac{\partial h}{\partial t}+U_2\frac{\partial h}{\partial x}$. Considering the stationary case (in which the displacement of the thrust pad along the vertical axis is zero) we can write:

$$V=\frac{dh}{dt}=\frac{\partial h}{\partial t}+U_2\frac{\partial h}{\partial x}=0 \iff \frac{\partial h}{\partial t}=-U_2\frac{\partial h}{\partial x} \quad (21)$$

Knowing that $\int_0^h\frac{\partial u}{\partial x}dy=\frac{\partial}{\partial x}\int_0^h u(y)\,dy-U_2\frac{\partial h}{\partial x}$, the speed can be integrated across the film thickness:

$$\int_0^h u(y)\,dy=-\frac{\phi}{\mu}\frac{\partial p}{\partial x}\left(2\frac{1-cosh(\omega h)}{\omega\,sinh(\omega h)}+h\right)+U_2\frac{cosh(\omega h)-1}{\omega\,sinh(\omega h)} \quad (22)$$

If $C=\frac{cosh(\omega h)-1}{\omega\,sinh(\omega h)}$, the mass conservation equation leads to a thin film equation describing the 1D flow in a porous medium:

$$\frac{\partial}{\partial x}\left(\frac{\phi}{\mu}(h-2C)\frac{\partial p}{\partial x}\right)=U_2\frac{\partial C}{\partial x}-U_2\frac{\partial h}{\partial x} \quad (23)$$

Generalization to a 2D flow is straightforward:

$$\frac{\partial}{\partial x}\left(\frac{\phi}{\mu}(h-2C)\frac{\partial p}{\partial x}\right)+\frac{\partial}{\partial z}\left(\frac{\phi}{\mu}(h-2C)\frac{\partial p}{\partial z}\right)=U_2\frac{\partial C}{\partial x}-U_2\frac{\partial h}{\partial x} \quad (24)$$

If the Brinkman term is ignored in equation (16) the Darcy Reynolds-type equation is:

$$\frac{\partial}{\partial x}\left(\frac{\phi}{\mu}h\frac{\partial p}{\partial x}\right)+\frac{\partial}{\partial z}\left(\frac{\phi}{\mu}h\frac{\partial p}{\partial z}\right)=-U_2\frac{\partial h}{\partial x} \quad (25)$$

### 4.2. Mathematical formulation of a Darcy- Forchheimer Reynolds-type equation

As shown in the paragraph 2.2, the flow within the porous medium can, for certain conditions, be better described by considering the Forchheimmer correction. In this case, the fluid velocity can be written in the following form:

$$u=-\frac{\phi^*(u)}{\mu}\frac{\partial p}{\partial x} \quad (26)$$

where $\phi^*$ can be considered as an apparent permeability which takes the following form:

$$\phi^*(u)=\frac{\mu\phi}{\mu+C_f\rho\sqrt{\phi}|u|} \quad (27)$$

Therefore, the Darcy- Forchheimer Reynolds-type equation is written in the following form:

$$\frac{\partial}{\partial x}\left(\frac{\phi^*}{\mu}h\frac{\partial p}{\partial x}\right)+\frac{\partial}{\partial z}\left(\frac{\phi^*}{\mu}h\frac{\partial p}{\partial z}\right)=-U_2\frac{\partial h}{\partial x} \quad (28)$$

as the apparent permeability $\phi^*$ depends on speed and thus pressure, an iterative algorithm is used to solve equation (28).

### 4.3. Numerical validation of the main assumptions

As mentioned previously, the XPHD lubrication model is based on a certain number of hypotheses that are usually used to describe thin-film flow. In order to verify the validity of our model, we compared our results with those obtained from commercial software (ABAQUS), which allows for a CFD calculation for the porous media. The model implemented in this software is very general, and is based on a combination of the Darcy-Brinkman-Forchheimer models:

$$\frac{\rho}{\varepsilon}\left(\frac{\partial u}{\partial t}+u\nabla\left(\frac{u}{\varepsilon}\right)\right)=-\nabla p+\frac{\mu}{\varepsilon}\nabla^2 u-\frac{\mu}{\phi}u-\frac{\rho C_f}{\sqrt{\phi}}|u|u \qquad (29)$$

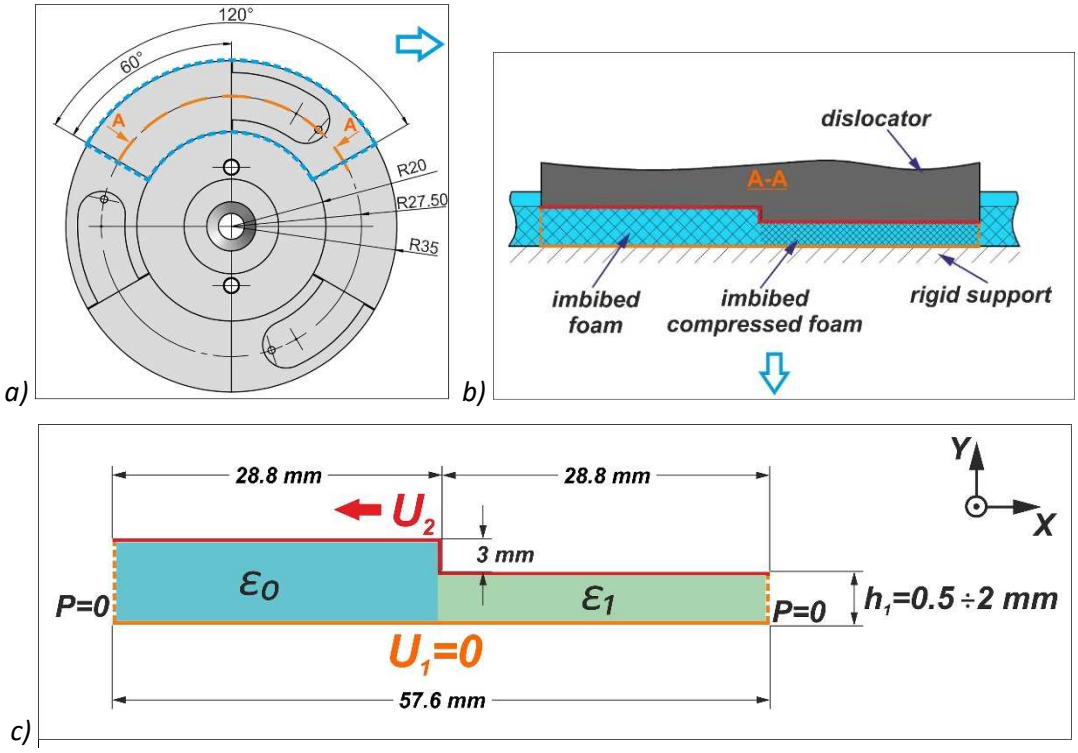


***Figure 21: Schema of ABAQUS model: a, b) cross section of a pad according to the mean radius; c) calculation domain (the pocket is omitted)***

Equation (29) represents an analogy to the Navier-Stokes equation. The CFD modeling presented below was carried out with a nil Forchheimer coefficient but also with $C_f=\frac{0.46}{\sqrt{\varepsilon^3}}$ . The calculations were carried out for a one-dimensional case. The geometry of the computational domain was as close as possible to the geometry of the pocketed dislocator used on the test bench (Figure 21).

As an example, Figure 22 shows the results of the CFD calculation for the case corresponding to a linear velocity of 864 mm/s (that corresponds to the linear velocity calculated at the average pad radius and a rotational speed of 300 rpm) and different values of $h_1$. It should be noted that the pressure is constant along the thickness of the foam, except for a zone with an abrupt change in thickness. Two flow directions can be distinguished: positive flow in the thin zone, and negative flow in the thick zone. In fact, unlike conventional lubrication, the displacement of the fluid inside the

porous medium is not due to the Couette effect (entrainment of the fluid by adhesion to the moving wall), but mainly due to compression of the structure induced by the movement of the dislocator.

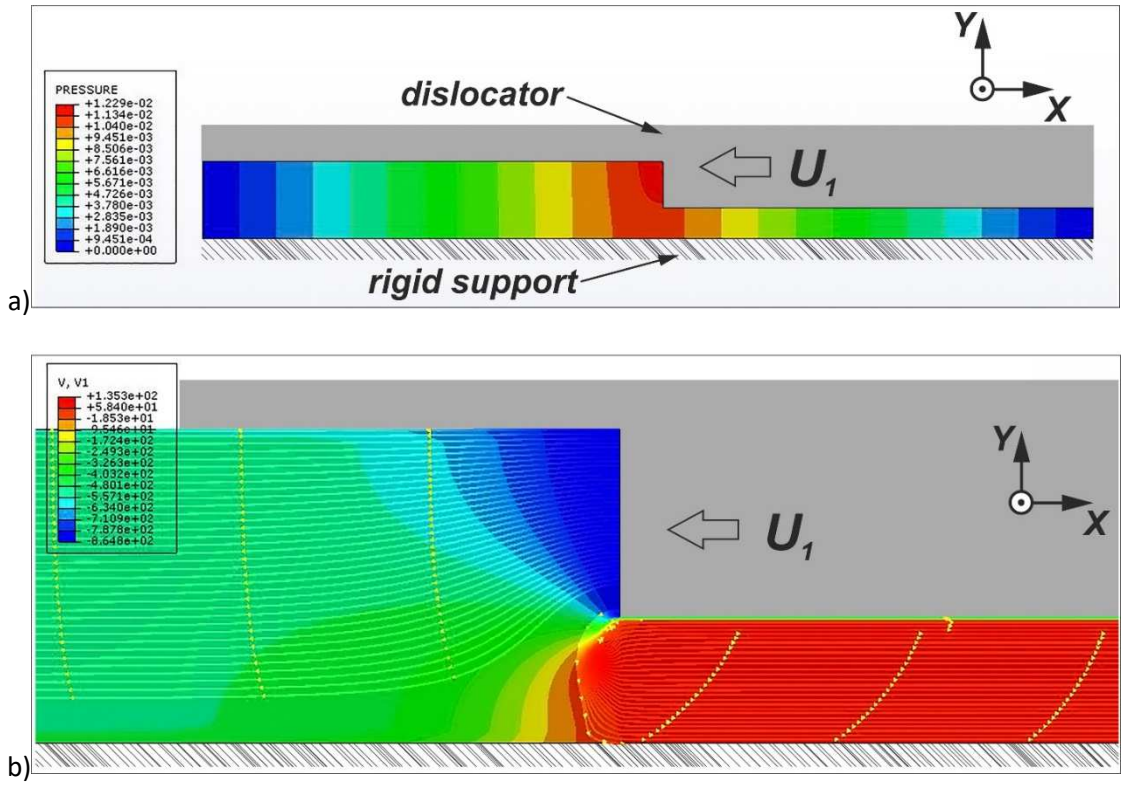


***Figure 22: Results for the CFD model (linear velocity 864 mm/s, $h_1$ = 2 mm): a) variation in pressure, b) variation in lubricant velocity along to $\vec{x}$ and streamlines***

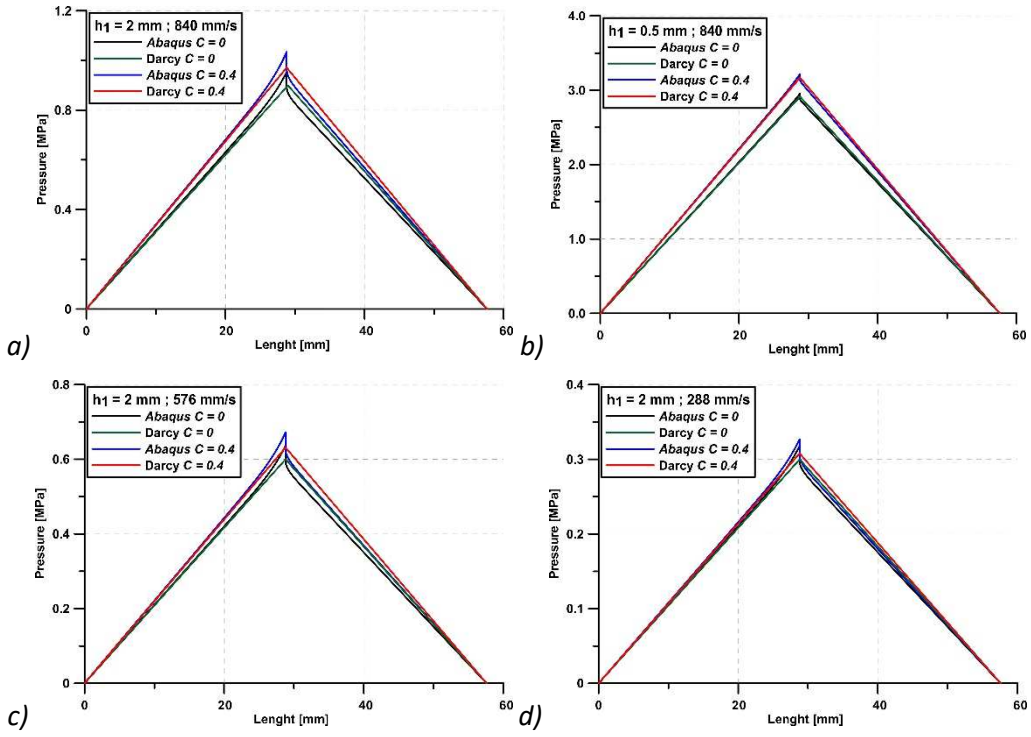


***Figure 23: Comparison of pressure variation obtained with CFD and XPHD models***

Figure 23 shows a comparison between the pressure variations obtained with the CFD and the XPHD lubrication models (Darcy and Darcy Brinkmann Reynolds type models give identical solutions). Good correlation can be seen except in the area of discontinuity in film thickness. It is also seen from Figure 23 that the abrupt variation in the geometry leads to local inertia effects that are not taken into account by the XPHD model. However, even in the worst case (Figure 23a), the differences remain negligible and localized. It can also be noted that taking into account the Forchheimer term slightly increases the maximum pressure although the differences between the CFD and the Reynolds models are still localized at the discontinuity point. It can therefore be concluded that the developed XPHD lubrication model is validated, at least for the operating conditions tested in this study.

# 5. Numerical results for XPHD thrust bearing

The purpose of this section is to try to reproduce numerically the experimental results obtained in Section 3. Results are presented for only three thicknesses of the compressed foam ($h_1$ = 1.6, 1.4 and 1.2 mm) lubricated with oil. An essential factor to consider in the modeling is the temperature of the oil during operation. The test bench did not allow the temperature of the tank to be controlled, but temperatures were measured on each pad of the dislocators. Figure 24 shows an example of temperatures measured as a function of speed for both dislocators. As can be seen, the temperature varies by a few degrees, and this result in variations in the dynamic viscosity, as shown in Figure 25 for all the cases studied in this section. The viscosity values shown in Figure 25 are used as input data for the numerical model.

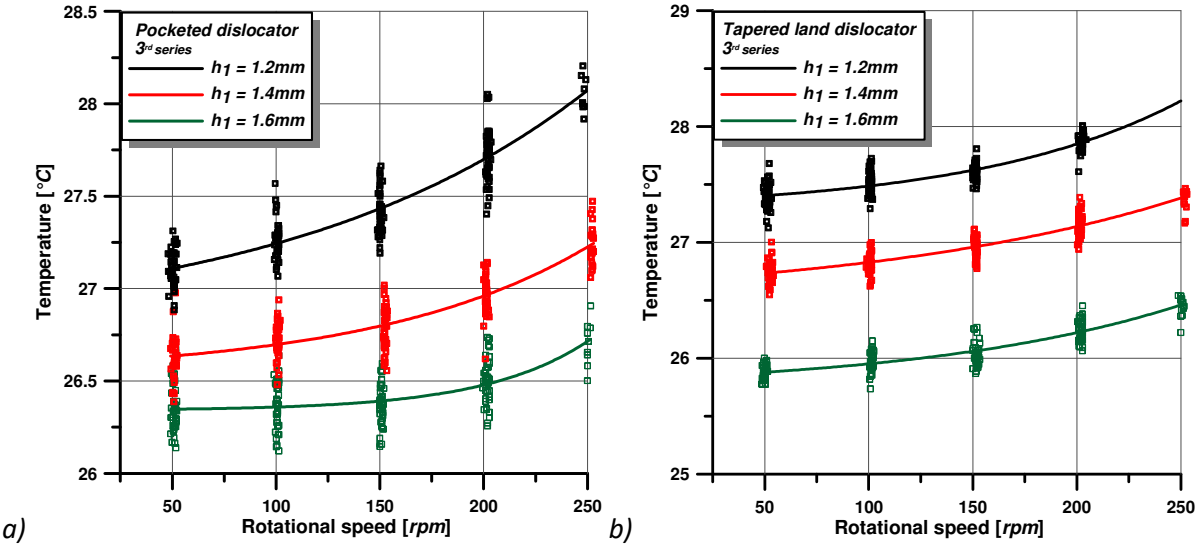


***Figure 24: Variation in the measured temperature with rotational speed***

The numerical modeling of the XPHD thrust bearings is based on equations (24) – Darcy Brinkman model and equation (25) - Darcy Forchheimer model[1], which were discretized using the finite element method. Calculations were performed for the imposed geometry and the dislocator was assumed to be perfectly parallel to the foam. The domain under study was therefore reduced to a single pad, with periodic boundary conditions in the circumferential direction.

The simplest way to predict the foam thickness after compression was to assume a perfect contact (i.e. with no gap) between the dislocator and the porous media. However, since the compression behavior law of the foam was known (see Section 2.3), a better approximation of the foam geometry was achieved by using Abaqus to simulate the deformation generated by the contact with the dislocator. Figure 26 shows a comparison between the foam geometry obtained with the two methods, for both dislocators. Differences can be observed at the sudden changes in the geometry of the dislocator, where the foam cannot remain in perfect contact, and small gaps appear.

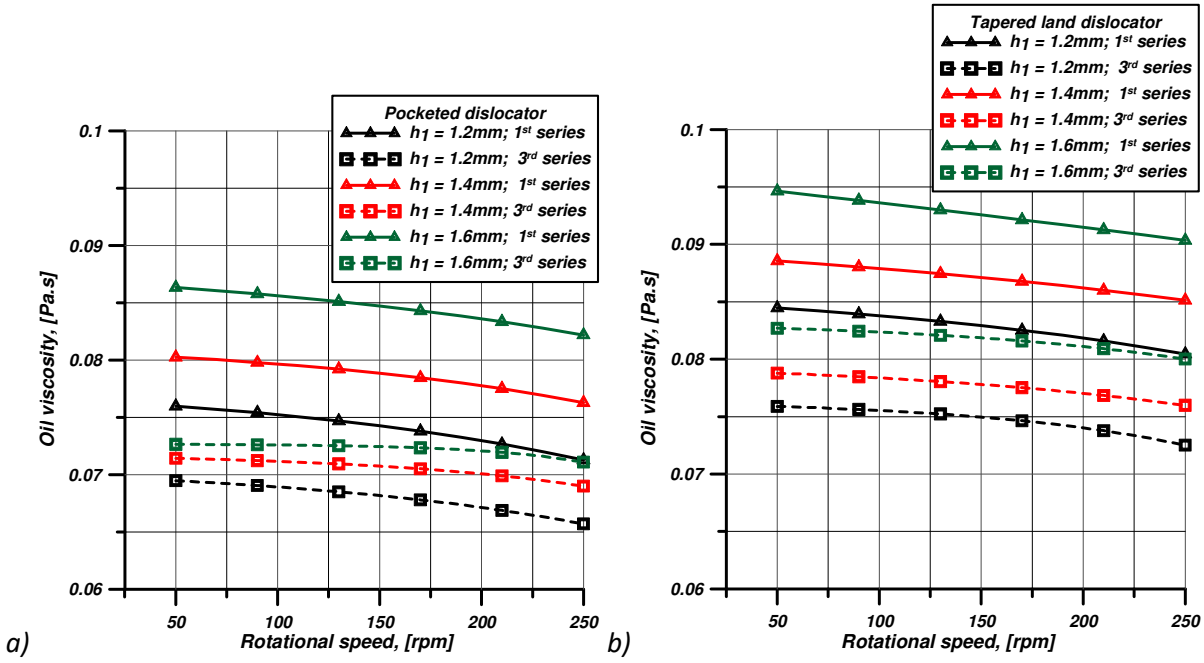


***Figure 25: Variation in dynamic viscosity as a function of speed and test series number***

As can be observed from Figure 27, the two methods of calculating the foam geometry give slightly different pressure fields. The hypothesis of perfect contact between the dislocator and the porous medium leads to an underestimation of the pressure, and consequently to a significant decrease in the bearing load capacity predicted by the model (see Figure 28). It can therefore be concluded that a theoretical estimation of the foam thickness should be avoided

[1] *The Darcy and Darcy-Brinkman models gave identical results for all operating conditions studied. Therefore, only the results with the Darcy-Brickman model are presented in this section.*

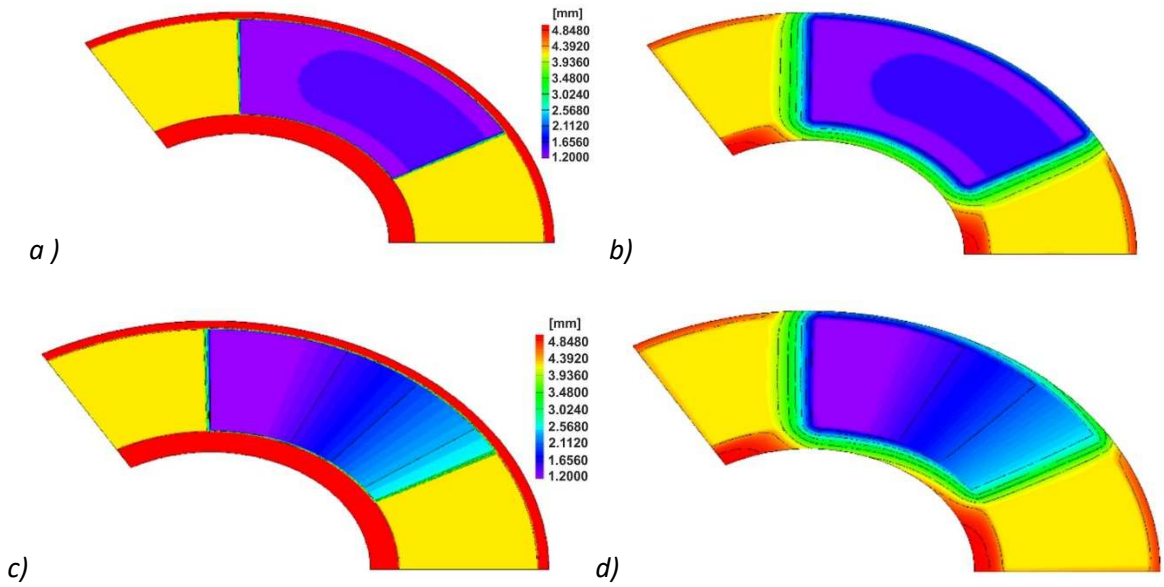


***Figure 26: Theoretical (a, c) and numerically determined (b, d) foam geometries for the pocketed (a, b) and tapered land (c, d) dislocators***

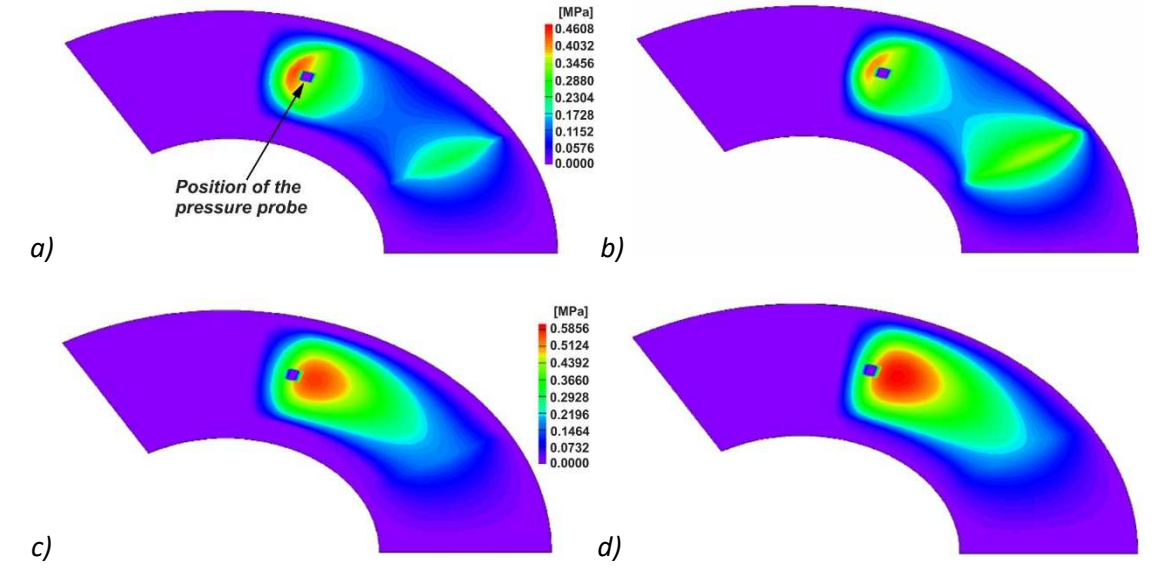


***Figure 27: Pressure fields calculated with theoretical (a, c) and numerically determined (b, d) foam geometries for the pocketed (a, b) and tapered land (c, d) dislocators ($h_1$ = 1.2 mm at 250 rpm); results obtained with the Darcy- Brinkman model***

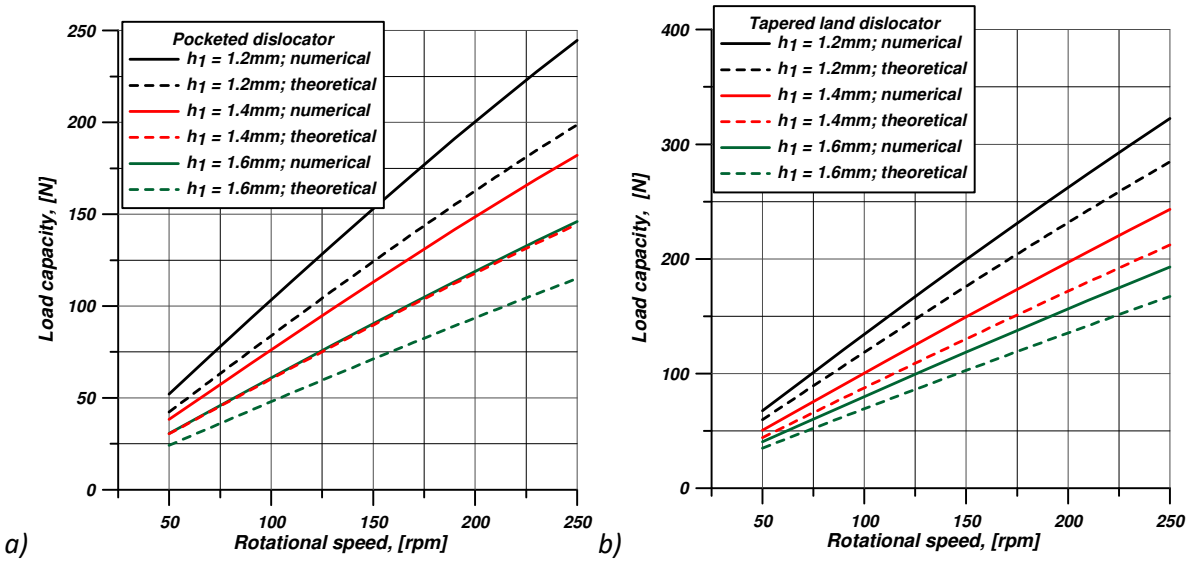


***Figure 28: Bearing load capacity calculated with theoretical and numerically determined foam geometries for the pocketed (a) and tapered land (d) dislocators; results obtained with the Darcy- Brinkman model***

Figure 29 shows a comparison between the experimentally measured and numerically predicted pressures for the pocketed (Figure 29 a) and tapered land (Figure 29 b) dislocators. Both Darcy and Darcy-Forchheimer models gave identical predictions. Overall, the comparisons are satisfactory for rotational speeds below 150 rpm. At higher speeds, the differences can be explained by imbibition problems that are not taken into account by the model, and which lead to a nonlinear variation in the pressure. The differences between the two measurement series can be explained by the difference in the operating temperature, and are not necessarily due to mechanical degradation of the foam.

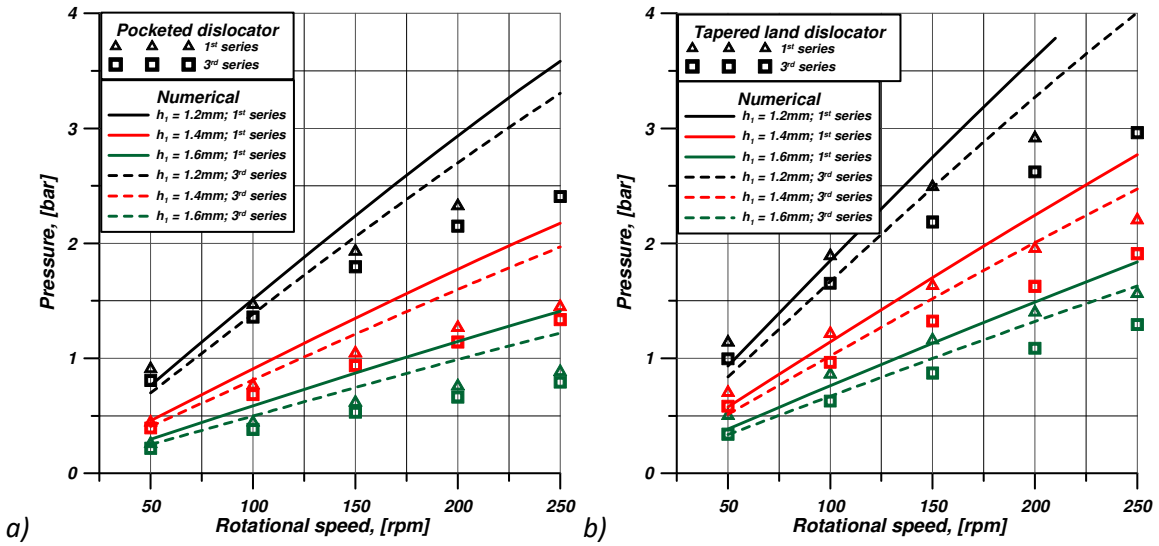


***Figure 29: Comparisons between experimentally measured and numerically predicted pressures***

In order to highlight the contribution of the Darcy-Forchheimer model, the pocketed bearing load capacity is is predicted for low speeds in Figure 30a) and for high speeds in Figure 30b). It can be

noted that for speeds below 250 rpm, there is no real difference between the two models. However, for speeds above 1000 rpm, the local inertia terms introduced by Forchheimer's model increase, as expected, the load capacity.

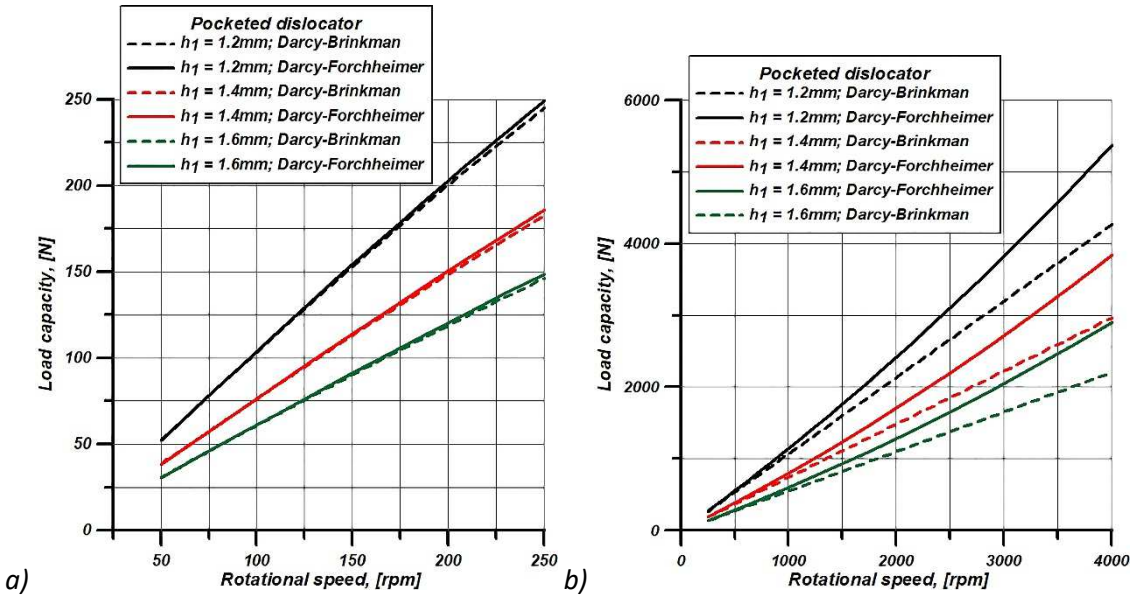


***Figure 30: : Bearing load capacity calculated with Darcy-Brinkman et Darcy-Forchheimer models***

The results presented in this section show that if used with care, the numerical model can predict the operation of an XPHD thrust bearing operating at low speed (<430 mm/s that corresponds to the linear velocity calculated at the average pad radius and a rotational speed of 150 rpm). However, it also highlights the need to take into account the foam dynamic imbibition phenomenon in order to be able to predict the behavior for higher rotational speeds.

# 6. Conclusions

This study represents a new step in the understanding of a new type of lubrication consisting of self-sustaining fluid films generated in highly compressible porous layers imbibed with liquids, referred to as XPHD lubrication by Prof. Pascovici.

In an initial characterization study, the essential parameters for XPHD lubrication were determined, including the porosity and permeability of the foam and its mechanical and geometrical properties. At the same time, we highlighted the difficulties encountered during the characterization of porous materials, an area that requires further work.

The second part of this paper focused on an experimental study of XPHD lubrication. An XPHD thrust bearing test facility allowed experimental investigations to be carried out in the imposed geometry mode, for rotational speeds of up to 250 rpm. It was shown that the performance of the system was highly dependent on the lubricant used, the re-imbibition capacity of the foam and the geometry of

the dislocator. In the general case, the pressure generated by the system tended to increase with the rotational speed and with a decrease in the thickness of the foam.

An XPHD lubrication model was also developed based on a Reynolds-type equation, derived from the Darcy-Brinkman-Forchheimer and the continuity equations. Our XPHD model was validated numerically for the operating conditions tested using the CFD module of a commercial software package. Comparisons of the modeling results with the test results showed that the model could predict the behavior of the XPHD thrust bearing at a relatively low rotational speeds (below 430 mm/s).

# 7. References


[1] Scheidegger AE. The physics of flow through porous media. 3rd ed. University of Toronto Press; 1974.

[2] Collins RE. Flow of fluids through porous materials. New York: Reinhold Publishing Corporation; 1961.

[3] Nield DA, Bejan A. Convection in porous media. 4th edition. New York: Springer; 2013. DOI: 10.1007/978-3-319-49562-0

[4] Pascovici MD. Lubrication by dislocation: A new mechanism for load carrying capacity. Proceedings of the 2nd World Tribology Congress, Vienna, p. 41-44, 2001.

[5] Pascovici MD .Procedure and device for pumping by fluid dislocation (Procedeu de pompare prin dislocarea fluidului si dispozitiv pentru realizarea acestuia). 1994, Romanian Patent 109469 (US 3794449).

[6] Pascovici MD, Cicone T. Squeeze-film of unconformal, compliant and layered contacts. Tribol. Int. 2003;36:791-799. DOI: 10.1016/S0301-679X(03)00095-1

[7] Pascovici MD, Cicone T, Marian V. G. Squeeze process under impact in highly compressible porous layers, imbibed with liquids. Tribol. Int. 2009;42:1433-1438. DOI: 10.1016/j.triboint.2009.05.006

[8] Pascovici MD. Lubrication of red blood cells in narrow capillaries. A heuristic approach. 2nd Vienna International Conference on Micro and Nano-Technology, p. 95-100, 2007.

[9] Han Y, Ganatos P, Weinbaum S. Transmission of steady and oscillatory fluid shear stress across epithelial and endothelial surface structures. Phys. Fluids 2005;17:1-13. DOI: 10.1063/1.1830485

[10] Feng J, Weinbaum S. Lubrication theory in highly compressible porous media: The mechanics of skiing, from red cells to humans. J. Fluid Mech. 2000;422:281-317. DOI: 10.1017/S0022112000001725

[11] Wu Q, Andreopoulos Y, Xanthos S, Weinbaum S. Dynamic compression of highly compressible porous media with application to snow compaction. J. Fluid Mech. 2005;542:281-304. DOI: 10.1017/S0022112005006294

[12] Wu Q, Igci Y, Andrepoulos Y, Weinbaum S. Lift mechanics of downhill skiing and snowboarding. ACSM J. Med. Sci. sports and exercises 2006;38 (6):1132-1146. DOI: 10.1249/01.mss.0000222842.04510.83

[13] Mirbod P, Andreopoulos Y, Weinbaum S. An airborne jet train that flies on a soft porous track. The American Physical Society, 61th Annual Meeting of the Division of Fluid Dynamics, San Antonio/Texas, 2008.

[14] Wu Q, Andreapoulos Y, Weinbaum S. From red cells to snowboarding: A new concept for a train track. Phys. Review Letters 2004;93:1-4. DOI: 10.1103/PhysRevLett.93.194501

[15] Weinbaum S, Andreopoulos Y, Mirbod P. Propulsion vehicle which travels along soft, porous track. Research Foundation of The City of New York. 2009, US 20110308422 A1.

[16] Dawson MA. Composite plates with a layer of fluid-filled, reticulated foam for blast protection of infrastructure. Int. J. Impact Eng. 2009;36:1288-1295. DOI: 10.1016/j.ijimpeng.2009.03.008
[17] Dawson MA, McKinley GH, Gibson LJ. The dynamic compressive response of open-cell foam impregnated with a Newtonian fluid. ASME J. Appl. Mech. 2008;75: 041015-1. DOI: 10.1115/1.2912940
[18] Dawson MA, McKinley GH, Gibson LJ. The dynamic compressive response of open-cell foam impregnated with a non-Newtonian fluid. ASME J. Appl. Mech. 2009;76: 061011-1 - 061011-8. DOI: 10.1115/1.3130825
[19] Gacka T, Zhu Z, Crawford R, Nathan R, Wu Q. From red cells to soft lubrication, an experimental study of lift generation inside a compressible porous layer. J. Fluid Mech. 2017;818:2-25. DOI: 10.1017/jfm.2017.133
[20] Zhu Z, Weinbaum S, Wu Q. Experimental study of soft porous lubrication. Phys. Review Fluids 2019;2: 1-6. DOI: 10.1103/PhysRevFluids.4.024305
[21] Zhu Z, Nathan R, Wu Q. An experimental study of the lubrication theory for highly compressible porous media, with and without lateral leakage. Tribol. Int. 2018;127:324-332. DOI: 10.1016/j.triboint.2018.06.016
[22] Wang Q, Nathan R, Wu Q. On fluid pressurization in a compressible porous media: A correction to the current theoretical models. J. Porous Media 2019;22(11): 1397-1410. DOI: 10.1615/JPorMedia.2019024717
[23] Lundström TS, Toll S, Håkanson JM. Measurement of the permeability tensor of compressed fibre beds. Transp. Porous Media 2002;47(3):363-380. DOI: 10.1023/A:1015511312595
[24] Turtoi P, Cicone T, Fatu A. Experimental and theoretical analysis of (water) permeability variation of nonwoven textiles subjected to compression. Mech. & Ind. 2017;18:307-8. DOI: 10.1051/meca/2016048
[25] Joseph DD, Nield DA, Papanicolaou G. Nonlinear Equation Governing Flow in a Saturated Porous Medium. Water Resources Research 1982;18(4):1049-1052, DOI: 10.1029/WR018i004p01049 and Correction 1983;19:591. DOI: 10.1029/WR019i002p00591
[26] Boomsma K, Poulikakos D. The effect of compression and pore size variations on the liquid flow characteristics in metal foams. J. Fluids Eng. 2002;124:263-272. DOI: 10.1115/1.1429637
[27] ISO 3386-1:1986. Polymeric materials, cellular flexible – Determination of stress-strain characteristics in compression – Part 1: Low-density materials
[28] https://classes.engineering.wustl.edu/2009/spring/mase5513/abaqus/docs/v6.6/books/usb/default.htm [accessed 20th December 2019].